Chen, Yixin, Decoupling Control of Flexure Jointed Hexapods, Ph.D, Department of Electrical and Computer Engineering, August, 2001.

As a member of the class of parallel manipulators, flexure jointed hexapods are great candidates for micro-precision applications in which only a very small workspace is required. This dissertation makes four major contributions to the research of flexure jointed hexapods. First, new decoupling algorithms are proposed. They exploit the properties of the joint space mass-inertia matrix of flexure jointed hexapods, loosen and remove the severe constraints imposed by previous methods on the allowable geometry, workspace, and payload. Second, a new identification algorithm is derived to estimate the joint space mass-inertia matrix, which plays a crucial role in the computation of decoupling transformations. The new identification algorithm, using an optimization criterion differing from the least squares criterion, also applies to a class of problems of estimating symmetric and positive definite matrices. Third, the relationships between different decoupling algorithms, disturbance rejection and robust stability is discussed. It is proven that optimal robustness can be achieved by choosing a unitary decoupling matrix. Finally, an approach for constructing optimal Jacobians for prioritized manipulations is described. A prioritized manipulation is a task in which some degrees of freedom (DOF) in the Cartesian space are more important than the rest. Thus the DOF can be divided into major DOF (MDOF) and secondary DOF (SDOF). Jacobians are constructed to achieve MDOFs while trading-off SDOFs with obstacle avoidance, fault tolerance, or joint motion optimization.

Contents

1 Introduction **1**
- 1.1 UW's Flexure Jointed Hexapods . . . 1
- 1.2 Dynamic Modeling of Flexure Jointed Hexapods . . . 4
- 1.3 Dissertation Organization . . . 8

2 Decoupling the Dynamics of Flexure Jointed Hexapods **11**
- 2.1 Constraints of the Prior Decoupling Methods . . . 11
- 2.2 Decoupling the Vibration Isolation Model . . . 13
  - 2.2.1 Simultaneous Diagonalization by Similarity . . . 14
  - 2.2.2 Simultaneous Diagonalization by Congruence . . . 16
- 2.3 Decoupling the Pointing Model . . . 19
- 2.4 Experimental Results . . . 21

3 Estimation of Symmetric, Positive Definite Matrices from Imperfect Measurements **27**
- 3.1 Related Work . . . 28
- 3.2 Problem Formulation . . . 30
- 3.3 Finding the Optimizer . . . 33
- 3.4 Numerical Results . . . 39

4 Decoupled Control **43**
- 4.1 Decoupling and Disturbance Rejection . . . 43
- 4.2 Decoupling and Robustness . . . 47
- 4.3 Unitary Decoupling and Optimal Robust Controller . . . 51

5 Optimal, Fault-Tolerant Velocity and Static Force Mapping for Prioritized Manipulation **53**
- 5.1 Differential Kinematics and Static Force Model . . . 55
  - 5.1.1 Nominal Model . . . 56
  - 5.1.2 Actuator Failures . . . 59
- 5.2 Optimal Velocity and Static Force Mapping . . . 63
  - 5.2.1 Trajectory Planning for Prioritized Manipulation . . . 63
  - 5.2.2 Isotropic Motion Planning . . . 70
- 5.3 Numerical Results . . . 74

6 Conclusions and Future Work **78**
6.1 Conclusions 78
6.2 Future Work 79

List of Figures

1.1 One of the UW's two flexure jointed hexapods. 2

1.2 Problem #1: Vibrating machinery must be isolated from a precision bus (this is termed the *dirty box* problem because the machinery mounted on the hexapod "box" is mechanically "dirty", i.e. vibrating). Problem #2: A precision payload must be manipulated in the presence of base vibrations and/or exogenous forces (this is termed the *quiet box* problem). 3

1.3 A flexure jointed hexapod (or Stewart Platform). $\{P\}$ is a Cartesian coordinate frame located at, and rigidly attached to, the payload's center of mass. $\{B\}$ is the frame attached to the (possibly moving) base, and $\{U\}$ is a Universal inertial frame of reference. 4

2.1 Using $\mathbf{J}^T$ as decoupling matrix. The payload's center of mass does not coincide with the center of the cube formed by six orthogonal struts. Bode magnitude plot and coherence from u_5 to $\vec{y}$. y_5 is denoted by "+" signs. . 23

2.2 Using $\mathbf{V}^T$ as decoupling matrix ($\mathbf{V}^T$ is calculated from $\mathbf{M}_p$). The payload's center of mass does not coincide with the center of the cube formed by six orthogonal struts. Bode magnitude plot and coherence from u_5 to $\vec{y}$. y_5 is denoted by "+" signs. 23

2.3 Using $\mathbf{V}^T$ as decoupling matrix ($\mathbf{V}^T$ is calculated from $\hat{\mathbf{M}}_p$). The payload's center of mass does not coincide with the center of the cube formed by six orthogonal struts. Bode magnitude plot and coherence from u_5 to $\vec{y}$. y_5 is denoted by "+" signs. 24

2.4 Using the first two columns of $\mathbf{J}$ as decoupling matrix. The payload's center of mass does not coincide with the center of the cube formed by six orthogonal struts. Bode magnitude plot and coherence from u_1 to $\vec{y}$. y_1 is denoted by "+" signs. 25

2.5 Using new decoupling matrix. The payload's center of mass does not coincide with the center of the cube formed by six orthogonal struts. Bode magnitude plot and coherence from u_1 to $\vec{y}$. y_1 is denoted by "+" signs. 26

3.1 Geometric interpretations of one parameter estimation using the least squares, the total least squares, and the new approaches. 31

3.2 Comparison of LS and SPDE methods: absolute mean and standard deviation of the estimation errors of $\mathbf{M}_p$'s entries. Mean{} and STD{} stand for the mean and the standard deviation, respectively. 41
3.3 Comparison of LS and SPDE methods: absolute mean and standard deviation of the estimation errors of $\mathbf{X}$'s entries. Mean{} and STD{} stand for the mean and the standard deviation, respectively. 42

4.1 A general closed-loop system. 44
4.2 A general decoupled control system. 46
4.3 A general closed-loop system with model perturbation. 48
4.4 A general decoupled control system with model perturbation. 49

5.1 Four legged fast steering mirror. 74

Chapter 1

Introduction

In various applications such as micro-manipulation, laser weapon pointing, space-based interferometers, reconnaissance cameras, optical and electron microscopy, optical communication, and remote sensing the presence of mechanical vibrations induced or transmitted in the system structure is almost inevitable. Consequently, the performance of the system depends critically on the ability of the existing sensor-actuator-controller architecture to provide vibration isolation and precise motion control. As great candidates for these applications, flexure jointed hexapods (Stewart Platform) can provide six degree-of-freedom (DOF) active and passive vibration isolation, six DOF high precision motion control, and fault tolerant vibration isolation and motion control (if less than six DOFs are required).

1.1 UW's Flexure Jointed Hexapods

Several researchers have developed flexure jointed hexapods for micro-precision applications in which only a very small workspace is required ([39], [37], [1], [11], [12], [36], [25], [32]). UW's hexapods are flexure jointed hexapods. Figure 1.1 shows the structure of

one of the UW's two flexure jointed hexapods. Like any hexapod, it consists of a base attached to a base plate, a payload plate, and six struts (also called legs). Each strut contains springs which passively reduce vibrations from the base to the payload plate. A voice coil motor is also embedded into each strut. Thus the hexapod can slightly change the length of it legs to allow additional active vibration reduction and precise pose control of the payload plate in up to six DOFs.

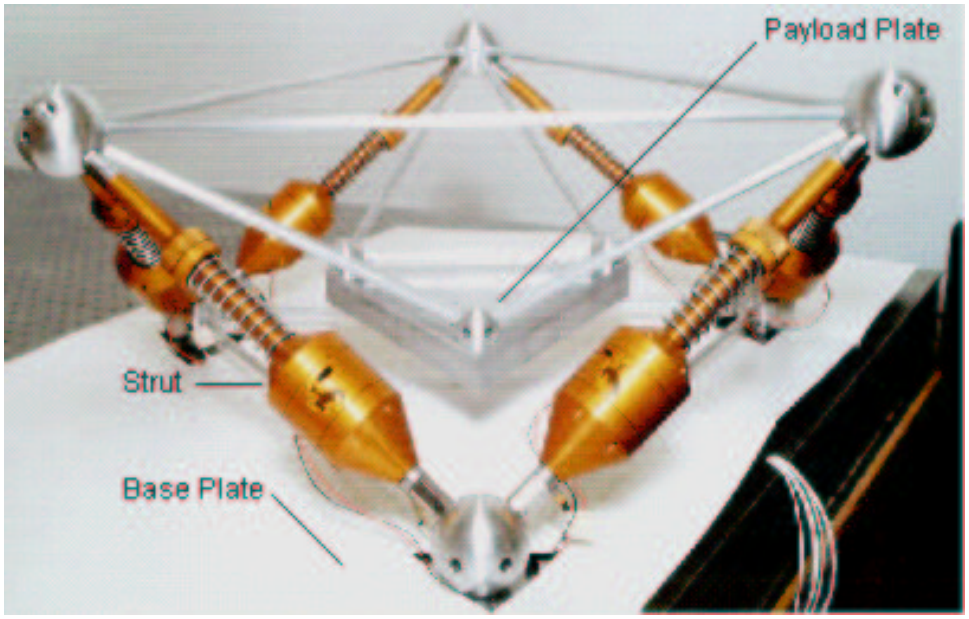

Figure 1.1: One of the UW's two flexure jointed hexapods.

Compared to non-flexure jointed hexapods, flexure jointed hexapods have several distinct characteristics [27]:

1. They employ flexure joints to avoid the extremely nonlinear micro-dynamics of joint friction and backlash. As a result, the flexures greatly alter the dynamic behavior.

2. The base motion is a significant contributor to the overall motion, even when the

base is subjected only to ambient seismic vibrations.

3. Because the workspace is so small, linearized dynamic models are highly accurate. This facilitates the analysis and design of the hexapod control system.

Problem #1: 6-Axis Vibration Isolation

Problem #2: 6-Axis Micro-Manipulation and Platform Stabilization

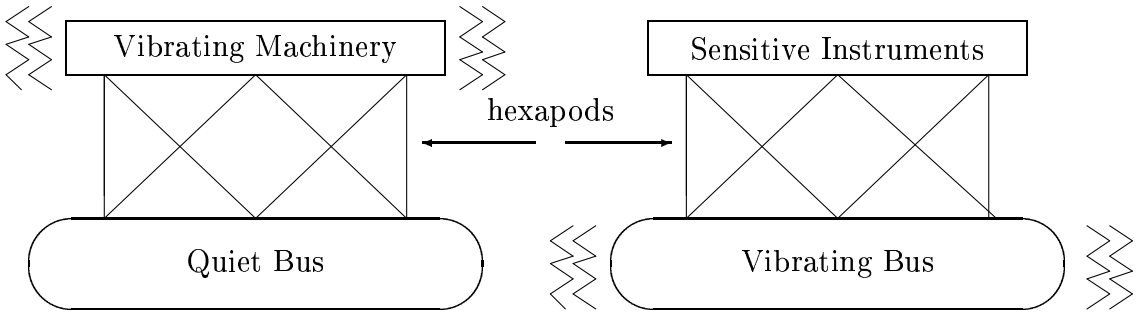

Figure 1.2: Problem #1: Vibrating machinery must be isolated from a precision bus (this is termed the *dirty box* problem because the machinery mounted on the hexapod "box" is mechanically "dirty", i.e. vibrating). Problem #2: A precision payload must be manipulated in the presence of base vibrations and/or exogenous forces (this is termed the *quiet box* problem).

For vibration isolation, flexure jointed hexapods have been developed to meet two principle needs, depending on what is mounted to the hexapod "box". Figure 1.2 defines the two general problems, namely the "quiet box" problem and the "dirty box" problem. Generally, the "quiet box" problem uses payload acceleration, velocity, or position measurements to control the payload motion. The "dirty box" problem uses base force feedback to minimize the transmission of forces to the base.

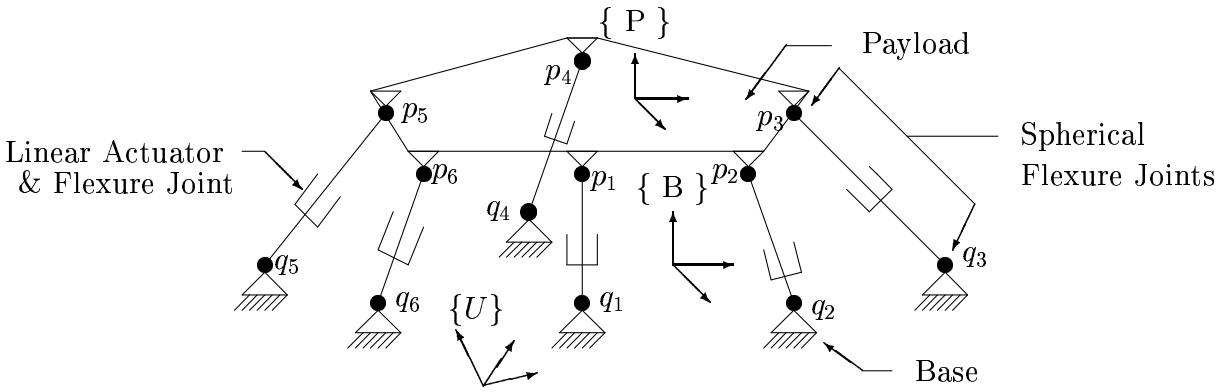

Figure 1.3: A flexure jointed hexapod (or Stewart Platform). $\{P\}$ is a Cartesian coordinate frame located at, and rigidly attached to, the payload's center of mass. $\{B\}$ is the frame attached to the (possibly moving) base, and $\{U\}$ is a Universal inertial frame of reference.

1.2 Dynamic Modeling of Flexure Jointed Hexapods

This section summarizes the dynamic models of flexure jointed hexapods [26] for vibration isolation and pointing purposes. Figure 1.3 illustrates the structural diagram of a general flexure jointed hexapod. Like any hexapod, it consists of a base, a payload, and six struts that can change their lengths using the linear actuators inside them. The struts, which have spherical joints at both ends, connect the payload to the base.

In the joint space, the dynamics of a flexure jointed hexapod are written as [26]

$$\vec{f}_b = \vec{f}_m - \mathbf{K}(\vec{l} - \vec{l}_r) - \mathbf{B}\dot{\vec{l}} \tag{1.1}$$

$$\begin{aligned}
&({}^U_P\mathbf{R}\,{}^P\mathbf{M}_x\,{}^B_P\mathbf{R}^T\mathbf{J}^{-1} + {}^U_B\mathbf{R}\mathbf{J}^T\mathbf{M}_s)\ddot{\vec{l}} + {}^U_B\mathbf{R}\mathbf{J}^T\mathbf{B}\dot{\vec{l}} + {}^U_B\mathbf{R}\mathbf{J}^T\mathbf{K}(\vec{l} - \vec{l}_r) = \\
&{}^U_B\mathbf{R}\mathbf{J}^T\vec{f}_m - ({}^U_B\mathbf{R}\mathbf{J}^T\mathbf{M}_s + {}^U_P\mathbf{R}\,{}^P\mathbf{M}_x\,{}^U_P\mathbf{R}^T\mathbf{J}_c\mathbf{J}_B{}^{-1})\ddot{\vec{q}}_s + \vec{\mathcal{F}}_e + \vec{\mathcal{G}} + \vec{\mathcal{C}}
\end{aligned} \tag{1.2}$$

where

- $\mathbf{J}$ is the 6×6 hexapod Jacobian relating payload Cartesian movements, expressed in the $\{P\}$ frame, to strut length changes in the joint space,
- ${}^{U}_{B}\mathbf{R}$ is the 6×6 rotation matrix from the base frame, $\{B\}$, to the Universal inertial frame of reference $\{U\}$ (it consists of two identical 3×3 rotation matrices forming a block diagonal 6×6 matrix). Similarly, ${}^{B}_{P}\mathbf{R}$ is the rotation matrix from the payload frame to the base frame, and ${}^{U}_{P}\mathbf{R} = {}^{U}_{B}\mathbf{R}\,{}^{B}_{P}\mathbf{R}$,
- $\mathbf{J}_c$ and $\mathbf{J}_B$ are 6×6 Jacobian matrices capturing base motion,
- ${}^{P}\mathbf{M}_x$ is the 6×6 mass-inertia matrix of the payload, found with respect to the payload frame, $\{P\}$, whose origin is at the hexapod payload's center of mass,
- $\mathbf{M}_s$ is a diagonal 6×6 matrix containing the moving mass of each strut,
- $\mathbf{B}$ and $\mathbf{K}$ are 6×6 diagonal matrices containing the damping and stiffness, respectively, of each strut,
- $\vec{l}$ is the 6×1 vector of strut lengths, and $\vec{l}_r$ is the constant vector of relaxed strut lengths,
- $\vec{f}_b$ is the 6×1 vector of forces exerted at the bottom of the strut,
- $\vec{f}_m$ is the 6×1 vector of strut motor forces,
- $\ddot{\vec{q}}_s$ is a 6×1 vector of base accelerations along each strut plus some Coriolis terms,
- $\vec{\mathcal{F}}_e$ is a 6×1 vector of payload exogenous generalized forces applied at the origin of the $\{P\}$ frame,

- $\vec{\mathcal{C}}$ is a 6×1 vector containing all the Coriolis and centripetal terms,

- $\vec{\mathcal{G}}$ is a 6×1 vector containing all gravity terms.

Since the struts can only move very small distances, the Jacobian ($\mathbf{J}$) and the rotation matrix (${}^{B}_{P}\mathbf{R}$) can be considered constant, and Coriolis and Centripetal terms are often negligible.

Note that the base motions play a role in the dynamic model (1.2) both explicitly ($\ddot{\vec{q}}_s$, ${}^{U}_{P}\mathbf{R}$, and ${}^{U}_{B}\mathbf{R}$) and implicitly (through $\ddot{\vec{l}}$, $\dot{\vec{l}}$, and $\vec{l}$). The relations among payload motion, base motion and strut dynamics can be described as [26]

$$\vec{l} = \vec{p}_s - \vec{q}_s \tag{1.3}$$

$$\dot{\vec{l}} = \dot{\vec{p}}_s - \dot{\vec{q}}_s \tag{1.4}$$

$$\ddot{\vec{l}} = \ddot{\vec{p}}_s - \ddot{\vec{q}}_s \tag{1.5}$$

where $\vec{p}_s = [\vec{u}_1^T\vec{p}_1, ..., \vec{u}_6^T\vec{p}_6]^T$, $\vec{q}_s = [\vec{u}_1^T\vec{q}_1, ..., \vec{u}_6^T\vec{q}_6]^T$, $\vec{p}_i$ denotes the three dimensional attachment point of the i^{th} strut to the payload and $\vec{q}_i$ denotes the attachment point of the i^{th} strut to the base (Figure 1.3), $\vec{u}_i$ is the unit direction vector of the i^{th} strut ($\vec{p}_i$, $\vec{q}_i$, and $\vec{u}_i$ are expressed in the same coordinate frame).

Substituting (1.3-1.5) into (1.1-1.2) and rearranging terms produces the following dynamic equations

$$\vec{f}_b = \vec{f}_m - \mathbf{K}(\vec{p}_s - \vec{q}_s - \vec{l}_r) - \mathbf{B}(\dot{\vec{p}}_s - \dot{\vec{q}}_s) \tag{1.6}$$

$$({}^{U}_{P}\mathbf{R}\,{}^{P}\mathbf{M}_x\,{}^{B}_{P}\mathbf{R}^T\mathbf{J}^{-1} + {}^{U}_{B}\mathbf{R}\mathbf{J}^T\mathbf{M}_s)\ddot{\vec{p}}_s + {}^{U}_{B}\mathbf{R}\mathbf{J}^T\mathbf{B}\dot{\vec{p}}_s + {}^{U}_{B}\mathbf{R}\mathbf{J}^T\mathbf{K}\vec{p}_s = {}^{U}_{B}\mathbf{R}\mathbf{J}^T\vec{f}_m +$$

$$({}^{U}_{P}\mathbf{R}\,{}^{P}\mathbf{M}_x\,{}^{B}_{P}\mathbf{R}^T\mathbf{J}^{-1} - {}^{U}_{P}\mathbf{R}\,{}^{P}\mathbf{M}_x\,{}^{U}_{P}\mathbf{R}^T\mathbf{J}_c\mathbf{J}_B{}^{-1})\ddot{\vec{q}}_s + {}^{U}_{B}\mathbf{R}\mathbf{J}^T\mathbf{B}\dot{\vec{q}}_s + {}^{U}_{B}\mathbf{R}\mathbf{J}^T\mathbf{K}(\vec{q}_s + \vec{l}_r) +$$

$$\vec{\mathcal{F}}_e + \vec{\mathcal{G}} + \vec{\mathcal{C}} \ . \tag{1.7}$$

For the small movements possible in flexure jointed hexapods, $\mathbf{J}$, $\mathbf{J}_c$, $\mathbf{J}_B$, and ${}^B_P\mathbf{R}$ are all nearly constant. For small base motions, ${}^U_B\mathbf{R}$, ${}^U_P\mathbf{R}$, and $\vec{\mathcal{G}}$ are constant, while $\vec{\mathcal{C}}$ can be neglected because large velocities cannot be attained in the small distance moved. Large base motions can be treated by incorporating ${}^U_B\mathbf{R}$ and feeding forward $\vec{\mathcal{G}}$ and $\vec{\mathcal{C}}$ terms.

By letting the spring compression absorb the static gravity forces (for small base motions) or the static part of gravity forces (for the large base motions), both $\vec{l}_r$ and $\vec{\mathcal{G}}$ terms can be removed. Thus (1.7) can be written as the following equation

$$\begin{aligned}
&({}^U_P\mathbf{R}^P\mathbf{M}_{x\,P}{}^B\mathbf{R}^T\mathbf{J}^{-1} + {}^U_B\mathbf{R}\mathbf{J}^T\mathbf{M}_s)\ddot{\vec{p}}_s + {}^U_B\mathbf{R}\mathbf{J}^T\mathbf{B}\dot{\vec{p}}_s + {}^U_B\mathbf{R}\mathbf{J}^T\mathbf{K}\vec{p}_s = {}^U_B\mathbf{R}\mathbf{J}^T\vec{f}_m + \\
&({}^U_P\mathbf{R}^P\mathbf{M}_{x\,P}{}^B\mathbf{R}^T\mathbf{J}^{-1} - {}^U_P\mathbf{R}^P\mathbf{M}_{x\,P}{}^U\mathbf{R}^T\mathbf{J}_c{\mathbf{J}_B}^{-1})\ddot{\vec{q}}_s + {}^U_B\mathbf{R}\mathbf{J}^T\mathbf{B}\dot{\vec{q}}_s + {}^U_B\mathbf{R}\mathbf{J}^T\mathbf{K}\vec{q}_s + \vec{\mathcal{F}}_e + \Delta\vec{\mathcal{G}}
\end{aligned} \tag{1.8}$$

where $\Delta\vec{\mathcal{G}}$ is the dynamic part of gravity forces. For small base motions, $\Delta\vec{\mathcal{G}} = \vec{0}$.

Multiplying both sides of (1.8) by $\mathbf{J}^{-T}{}^U_B\mathbf{R}^T$, we get

$$\mathbf{M}_p\ddot{\vec{p}}_s + \mathbf{B}\dot{\vec{p}}_s + \mathbf{K}\vec{p}_s = \vec{f}_m + \mathbf{M}_q\ddot{\vec{q}}_s + \mathbf{B}\dot{\vec{q}}_s + \mathbf{K}\vec{q}_s + \mathbf{J}^{-T}{}^U_B\mathbf{R}^T(\vec{\mathcal{F}}_e + \Delta\vec{\mathcal{G}}) \tag{1.9}$$

where

$$\mathbf{M}_p = \mathbf{J}^{-T}{}^B_P\mathbf{R}^P\mathbf{M}_{x\,P}{}^B\mathbf{R}^T\mathbf{J}^{-1} + \mathbf{M}_s \tag{1.10}$$

$$\mathbf{M}_q = \mathbf{J}^{-T}{}^B_P\mathbf{R}^P\mathbf{M}_{x\,P}{}^B\mathbf{R}^T\mathbf{J}^{-1} - \mathbf{J}^{-T}{}^B_P\mathbf{R}^P\mathbf{M}_{x\,P}{}^U\mathbf{R}^T\mathbf{J}_c{\mathbf{J}_B}^{-1}. \tag{1.11}$$

Thus the dynamic model for vibration isolation ("quiet box" and "dirty box") is given by (1.6) and (1.9).

Let

$$\vec{\chi} = [\theta_x, \theta_y, \theta_z, T_x, T_y, T_z]^T \tag{1.12}$$

represent the Cartesian space movements (rotation and translation) of the payload plate. θ_x, θ_y, and θ_z are the amount of rotation along x, y, and z axis, respectively. T_x, T_y, and T_z are the amount of translation along x, y, and z axis, respectively. Then the dynamic model for pointing is

$$\vec{\chi} = \mathbf{J}^{-1}(\mathbf{M}_p s^2 + \mathbf{B}s + \mathbf{K})^{-1}\vec{f}_m. \tag{1.13}$$

In many pointing applications, only part of the six DOFs are needed. For example, only θ_x and θ_y are the pointing DOFs for the UW's hexapod. In this case, the dynamic model can be written as

$$\vec{\chi}_a = \begin{bmatrix} 1 & 0 & 0 & 0 & 0 & 0 \\ 0 & 1 & 0 & 0 & 0 & 0 \end{bmatrix} \mathbf{J}^{-1}(\mathbf{M}_p s^2 + \mathbf{B}s + \mathbf{K})^{-1}\vec{f}_m \tag{1.14}$$

where $\vec{\chi}_a = \begin{bmatrix} \theta_x \\ \theta_y \end{bmatrix}$.

1.3 Dissertation Organization

The remainder of this dissertation is organized as follows:

- **Chapter 2. Decoupling the Dynamics of Flexure Jointed Hexapods**

  By exploiting properties of the joint space mass-inertia matrix of flexure jointed hexapods, new decoupling methods are proposed. The new decoupling methods, through a static input-output mapping, transform the highly coupled system

dynamics into independent single-input single-output (SISO) channels. Controls for these SISO channels are far simpler than their multiple-input multiple-output (MIMO) counterparts while facilitating advanced control features such as adaptation, fault tolerant, iterative learning, etc. Prior decoupling control methods imposed severe constraints on the allowable geometry, workspace, and payload. The new methods loosen and remove these constraints, thus greatly expanding the applications.

- **Chapter 3. Estimation of Symmetric, Positive Definite Matrices from Imperfect Measurements**

  To apply the decoupling algorithms proposed in Chapter 2, the joint space mass-inertia matrix ($\mathbf{M}_p$) of the flexure jointed hexapod must be known. There are two ways of obtaining $\mathbf{M}_p$. One way is to calculate $\mathbf{M}_p$ from the design parameters of the hexapod. The other is to identify $\mathbf{M}_p$ from measurements. The former method requires exact values of $\mathbf{M}_s$, ${}^{P}\mathbf{M}_x$, ${}^{B}_{P}\mathbf{R}$, and $\mathbf{J}$, which in practice are laborious to compute and can introduce errors. In this chapter, a new identification algorithm is proposed to directly estimate $\mathbf{M}_p$ from noisy measurements. The algorithm applies to a class of problems for estimating symmetric and positive definite matrices.

- **Chapter 4. Decoupled Control**

  In this chapter, we first discuss the relationships between different decoupling algorithms and the disturbance rejection performance of the corresponding closed-loop systems. Then, we briefly summarize the robust stability test for several

perturbation models. Finally, we show that optimal robustness can be achieved by choosing a unitary decoupling matrix.

- **Chapter 5. Optimal, Fault Tolerant Velocity and Static Force Mapping for Prioritized Manipulation**

  In many applications, some DOFs in the Cartesian space (operational space) are more important than the rest in performing a task. For example, the rotations along the x and y axes are the major concern for a pointing task, while rotation along the z axis and translations have almost no influence on the pointing performance. When pointing a camera at distant objects, orientation of the camera is more important than position. In welding, rotations about the welding rod may be irrelevant. We call these applications prioritized manipulation. The end-effector's DOFs during a prioritized manipulation can be divided into major DOFs (MDOFs) and secondary DOFs (SDOFs). MDOFs are more important than SDOFs in performing a task. In this chapter, we describe an approach for sacrificing the SDOFs for some particular reasons such as avoiding obstacles in the workspace, optimizing certain kinematic performance indices, or tolerating actuator failures, etc.

- **Chapter 6. Conclusions and Future Work**

  We summarize the main contributions of our research, and discuss how the results might be improved by future work.

Chapter 2

Decoupling the Dynamics of Flexure Jointed Hexapods

This chapter first discusses three constraints imposed by the prior decoupling algorithms [27]. Then, we introduce new decoupling methods that relax the first constraint and remove the remaining constraints.

2.1 Constraints of the Prior Decoupling Methods

McInroy, et al. [27] proposed two decoupling algorithms, using $\mathbf{J}^T$ or $\mathbf{J}^{-1}$ as decoupling transformations, which can be used in the "quiet box" problem (using payload acceleration, velocity, or position measurements to control the payload motion) and the "dirty box" problem (using base force feedback to minimize the transmission of forces to the base). However three conditions must be met in order to make the algorithms apply:

- The strut mass, damping, and stiffness matrices are scaled identities, $\mathbf{M}_s = m\mathbf{I}$, $\mathbf{B} = b\mathbf{I}$, $\mathbf{K} = k\mathbf{I}$.
- The payload mass-inertia matrix (${}^B\mathbf{M}_x$) found with respect to the base frame $\{B\}$ is diagonal.

- $\mathbf{J}^T\mathbf{J}$ is diagonal over the whole workspace.

The first condition is easily satisfied whenever the struts are identical in construction (they may differ in length) which is true and desirable for many applications. But there are some applications that require different strut properties. For instance, in some hexapods, three struts contributing to the translating movements are identical, and the remaining three contributing to the rotating movements are also identical. But the strut properties are different between the two groups. In this case, $\mathbf{M}_s$, $\mathbf{B}$, and $\mathbf{K}$ are only diagonal.

The second condition is slightly more restrictive. The payload mass-inertia matrix ($^B\mathbf{M}_x$), found with respect to the base frame $\{B\}$, consists of two blocks, one expressing mass and the other expressing inertial properties of the payload,

$$\begin{aligned} {}^B\mathbf{M}_x &= {}^B_P\mathbf{R}\,{}^P\mathbf{M}_x\,{}^B_P\mathbf{R}^T \\ &= \begin{bmatrix} m_p\mathbf{I}_{3\times3} & \mathbf{0}_{3\times3} \\ \mathbf{0}_{3\times3} & {}^B_P\mathbf{R}\,{}^c\mathbf{I}^B_P\mathbf{R}^T \end{bmatrix} \end{aligned} \tag{2.1}$$

where m_p is the payload mass, and $^c\mathbf{I}$ is the inertia tensor [7] of the payload with respect to the payload frame $\{P\}$. The upper block, $m_p\mathbf{I}_{3\times3}$, is always diagonal. The lower block, ${}^B_P\mathbf{R}\,{}^c\mathbf{I}^B_P\mathbf{R}^T$, can be diagonal if there exists three orthogonal axes of symmetry with the payload mass distributed symmetrically about these axes. It is then diagonal if $\{B\}$ is selected to have the same orientation as these axes. This condition can be satisfied as long as the payload is a fixed rigid body. In this dissertation, the payload is supposed to be a fixed rigid body. This assumption is made partly to simplify the approach and partly because all known flexure jointed hexapods satisfy this constraint. Thus this

condition can usually be satisfied, although finding the principal axes of a payload is laborious, especially when the payload changes often.

The last condition is by far the most restrictive. It relies heavily on the hexapod geometric design. Three hexapod configurations satisfying the geometry requirements are proposed in [27]. In all of these configurations, the payload's center of mass must be placed in some position determined by the corresponding hexapod geometry since the Jacobian, $\mathbf{J}$, is a function of the payload's center of mass. Thus any changes to the payload require at least the tedious procedure of computing and adjusting the position of the payload's center of mass by adding or reducing some counterweights. Furthermore, this constraint significantly limits the location of the end effector, thus eliminating many important applications. For example, the close quarters required for dual hexapods performing micro-manipulation tasks prohibit the mass balancing required by earlier methods.

2.2 Decoupling the Vibration Isolation Model

The new decoupling algorithm is based on the simultaneous diagonalization of $\mathbf{M}_p$, $\mathbf{B}$, and $\mathbf{K}$ matrices. Instead of being scaled identities, $\mathbf{M}_s$, $\mathbf{B}$ and $\mathbf{K}$ are only required to be diagonal matrices satisfying $\mathbf{B} = \alpha\mathbf{K}$, where α is a nonzero scalar constant. In addition, the remaining much more restrictive conditions are removed. The algorithm is suitable for both the "quiet box" and "dirty box" problems.

2.2.1 Simultaneous Diagonalization by Similarity

First, let's consider the case where $\mathbf{B}$ and $\mathbf{K}$ are scaled identities ($\mathbf{B}$ does not necessarily equal $\mathbf{K}$). This happens when all six struts of the hexapod are identical in damping and stiffness, while they may be different in mass and length.

From (2.1), it is easily seen that ${}^{B}\mathbf{M}_x$ is symmetric. This implies that

$$\begin{aligned} \mathbf{M}_p{}^T &= (\mathbf{J}^{-1})^T {}^{B}\mathbf{M}_x{}^T (\mathbf{J}^{-T})^T + \mathbf{M}_s{}^T \\ &= \mathbf{J}^{-T\,B}\mathbf{M}_x\mathbf{J}^{-1} + \mathbf{M}_s \\ &= \mathbf{M}_p \ . \end{aligned} \tag{2.2}$$

Hence the joint space mass-inertia matrix $\mathbf{M}_p$ is symmetric. Thus it can be unitarily diagonalized using the Schur Decomposition [13]

$$\mathbf{M}_p = \mathbf{V}\mathbf{D}\mathbf{V}^T \tag{2.3}$$

where $\mathbf{V}$ is an orthogonal matrix ($\mathbf{V}\mathbf{V}^T = \mathbf{V}^T\mathbf{V} = \mathbf{I}$), and $\mathbf{D}$ is a diagonal matrix. Clearly, $\mathbf{V}^T\mathbf{M}_p\mathbf{V} = \mathbf{D}$, $\mathbf{V}^T\mathbf{B}\mathbf{V} = \mathbf{B}$, $\mathbf{V}^T\mathbf{K}\mathbf{V} = \mathbf{K}$ are simultaneously diagonalized.

For the "quiet box" problem, the dynamic model is described by equation (1.9). Define a new input and a new output by

$$\vec{u} = \mathbf{V}^T \vec{f}_m \tag{2.4}$$

$$\vec{y} = \mathbf{V}^T \vec{p}_s \, . \tag{2.5}$$

Then (1.9) can be written as

$$\mathbf{D}\ddot{\vec{y}} + \mathbf{B}\dot{\vec{y}} + \mathbf{K}\vec{y} = \vec{u} + \mathbf{V}^T(\mathbf{M}_q\ddot{\vec{q}}_s + \mathbf{B}\dot{\vec{q}}_s + \mathbf{K}\vec{q}_s) + \mathbf{V}^T\mathbf{J}^{-T\,U}_{\ B}\mathbf{R}^T\vec{\mathcal{F}}_e \, . \tag{2.6}$$

Note that $\mathbf{D}$, $\mathbf{B}$, and $\mathbf{K}$ matrices are diagonal. Consequently, the dynamics from $\vec{u}$ to $\vec{y}$ are LTI decoupled, and independent SISO controls can be designed. In addition to simplifying nominal control design, this also facilitates fault tolerant controls [25]. Based on (2.6), SISO LTI control algorithms can be designed to suppress the base movement ($\ddot{\vec{q}}_s$, $\dot{\vec{q}}_s$, and $\vec{q}_s$) and exogenous force ($\vec{\mathcal{F}}_e$) influences on the payload.

For "dirty box" vibration isolation applications, base forces are typically fed back, rather than payload positions, velocities or accelerations. Assuming the base is stationary or can only move over small ranges, i.e., $\mathbf{M}_q$ and ${}^{U}_{B}\mathbf{R}$ in (1.9) can be regarded as constant matrices. The algorithm may be re-formulated to cover "dirty box" problems as follows. First, substituting (1.6) into (1.9), assuming $\vec{l_r}$ and $\vec{\mathcal{G}}$ terms cancel each other (because of small base movements), and solving for $\vec{f_b}$ gives

$$\vec{f_b} = \mathbf{M}_p \ddot{\vec{p}}_s - \mathbf{M}_q \ddot{\vec{q}}_s - \mathbf{J}^{-T} {}^{U}_{B}\mathbf{R}^T \vec{\mathcal{F}}_e \ . \tag{2.7}$$

Since $\mathbf{M}_q$ and ${}^{U}_{B}\mathbf{R}$ are constant, equations (1.9) and (2.7) are LTI. Thus Laplace transforms can be taken to yield

$$\vec{f_b} = \mathbf{M}_p s^2 \vec{p}_s - \mathbf{M}_q s^2 \vec{q}_s - \mathbf{J}^{-T} {}^{U}_{B}\mathbf{R}^T \vec{\mathcal{F}}_e \tag{2.8}$$

$$(\mathbf{M}_p s^2 + \mathbf{B}s + \mathbf{K})\vec{p}_s = \vec{f_m} + (\mathbf{M}_q s^2 + \mathbf{B}s + \mathbf{K})\vec{q}_s + \mathbf{J}^{-T} {}^{U}_{B}\mathbf{R}^T \vec{\mathcal{F}}_e \, . \tag{2.9}$$

Then inserting (2.8) into (2.9) and rearranging terms yields

$$\begin{aligned} \vec{f_b} = {} & \mathbf{M}_p s^2 (\mathbf{M}_p s^2 + \mathbf{B}s + \mathbf{K})^{-1} \vec{f_m} - \mathbf{M}_q s^2 \vec{q}_s + \\ & \mathbf{M}_p s^2 (\mathbf{M}_p s^2 + \mathbf{B}s + \mathbf{K})^{-1} (\mathbf{M}_q s^2 + \mathbf{B}s + \mathbf{K}) \vec{q}_s + \\ & [\mathbf{M}_p s^2 (\mathbf{M}_p s^2 + \mathbf{B}s + \mathbf{K})^{-1} - \mathbf{I}] \mathbf{J}^{-T} {}^{U}_{B}\mathbf{R}^T \vec{\mathcal{F}}_e \ . \end{aligned} \tag{2.10}$$

Define a new input and a new output

$$\vec{u} = \mathbf{V}^T \vec{f}_m \tag{2.11}$$

$$\vec{y} = \mathbf{V}^T \vec{f}_b \tag{2.12}$$

where $\mathbf{V}$ is defined by (2.3). Then (2.10) becomes

$$\begin{aligned}\vec{y} = \mathbf{D}s^2(\mathbf{D}s^2 + \mathbf{B}s + \mathbf{K})^{-1}\vec{u} - \mathbf{V}^T\mathbf{M}_q s^2 \vec{q}_s + \\ \mathbf{D}s^2(\mathbf{D}s^2 + \mathbf{B}s + \mathbf{K})^{-1}\mathbf{V}^T(\mathbf{M}_q s^2 + \mathbf{B}s + \mathbf{K})\vec{q}_s + \\ [\mathbf{D}s^2(\mathbf{D}s^2 + \mathbf{B}s + \mathbf{K})^{-1} - \mathbf{I}]\mathbf{V}^T\mathbf{J}^{-T}{}_B^U\mathbf{R}^T\vec{\mathcal{F}}_e \ .\end{aligned} \tag{2.13}$$

Since $\mathbf{D}s^2(\mathbf{D}s^2 + \mathbf{B}s + \mathbf{K})^{-1}$ is a diagonal transfer function matrix, once again, the dynamics from $\vec{u}$ to $\vec{y}$ are decoupled. SISO LTI compensators from $\vec{u}$ to $\vec{y}$ can be designed to suppress the base acceleration and exogenous force disturbances. Note that this can be viewed in two ways. If $\vec{\mathcal{F}}_e$ is the dominant disturbance, then the control provides dirty box isolation. If $\vec{q}_s$ is the dominant disturbance, then the hexapod attempts to quiet a vibrating structure.

2.2.2 Simultaneous Diagonalization by Congruence

In some applications, the struts have different physical properties, i.e., $\mathbf{M}_s$, $\mathbf{B}$, and $\mathbf{K}$ matrices are only diagonal (not necessarily identities). Thus the algorithms in section 2.2.1 are no longer valid. However, if the $\mathbf{B}$ and $\mathbf{K}$ are symmetric and satisfy the condition $\mathbf{B} = \alpha\mathbf{K}$ where α is a nonzero scalar constant, then $\mathbf{M}_p$, $\mathbf{B}$, and $\mathbf{K}$ matrices can still be simultaneously diagonalized.

Equation (2.2) shows that $\mathbf{M}_p$ is symmetric. In fact, $\mathbf{M}_p$ is also positive definite. This fact comes from the intrinsic physical properties of the $\mathbf{M}_p$ matrix. The kinetic energy of the payload is defined by

$$K_e = \frac{1}{2}\dot{\vec{\chi}}^T \mathbf{M}_p \dot{\vec{\chi}} \tag{2.14}$$

where K_e is the kinetic energy of the payload, $\dot{\vec{\chi}}$ is the payload's generalized, or spatial velocity. Since $K_e > 0$ for all $\dot{\vec{\chi}} \neq \vec{0}$, it can be concluded that $\mathbf{M}_p$ is positive definite.

Since $\mathbf{M}_p$ is positive definite and $\mathbf{B}$ is symmetric, there exists a nonsingular matrix $\mathbf{C}$ such that $\mathbf{C}^T\mathbf{M}_p\mathbf{C}$ and $\mathbf{C}^T\mathbf{B}\mathbf{C}$ are both diagonal [16]. Moreover, $\mathbf{C}$ can be calculated as follows. First, calculate the Schur decomposition of $\mathbf{M}_p$, which is given by (2.3). Since $\mathbf{M}_p$ is positive definite, all the diagonal entries of $\mathbf{D}$ are positive. Next, define a new matrix by

$$\mathbf{B}_1 = \mathbf{D}^{-\frac{1}{2}}\mathbf{V}^T\mathbf{B}\mathbf{V}\mathbf{D}^{-\frac{1}{2}}. \tag{2.15}$$

It is obvious that $\mathbf{B}_1$ is symmetric, thus the Schur decomposition is given by

$$\mathbf{B}_1 = \mathbf{U}\mathbf{\Lambda}\mathbf{U}^T \tag{2.16}$$

where $\mathbf{U}$ is an orthogonal matrix and $\mathbf{\Lambda}$ is a diagonal matrix. Finally, the simultaneous diagonalization matrix, which is invertible, is given by

$$\mathbf{C} = \mathbf{V}\mathbf{D}^{-\frac{1}{2}}\mathbf{U} \ . \tag{2.17}$$

It can be easily shown that $\mathbf{C}^T\mathbf{M}_p\mathbf{C} = \mathbf{I}$ and $\mathbf{C}^T\mathbf{B}\mathbf{C} = \mathbf{\Lambda}$. Furthermore, if $\mathbf{B} = \alpha\mathbf{K}$, then $\mathbf{C}^T\mathbf{K}\mathbf{C} = \frac{1}{\alpha}\mathbf{\Lambda}$. Thus, $\mathbf{C}$ simultaneously diagonalizes $\mathbf{M}_p$, $\mathbf{B}$, and $\mathbf{K}$ matrices.

For the "quiet box" problem, a new input and a new output are defined by

$$\vec{u} = \mathbf{C}^T \vec{f}_m \tag{2.18}$$

$$\vec{y} = \mathbf{C}^{-1} \vec{p}_s \,. \tag{2.19}$$

Then (1.9) can be written as

$$\ddot{\vec{y}} + \mathbf{\Lambda}\dot{\vec{y}} + \frac{1}{\alpha}\mathbf{\Lambda}\vec{y} = \vec{u} + \mathbf{C}^T \mathbf{J}^{-T} {}^{U}_{B}\mathbf{R}^T \vec{\mathcal{F}}_e + \mathbf{C}^T(\mathbf{M}_q \ddot{\vec{q}}_s + \mathbf{B}\dot{\vec{q}}_s + \mathbf{K}\vec{q}_s) \,. \tag{2.20}$$

The dynamics from $\vec{u}$ to $\vec{y}$ are LTI decoupled. Based on (2.20), SISO LTI control algorithms can be designed to suppress the base movement ($\ddot{\vec{q}}_s$, $\dot{\vec{q}}_s$, and $\vec{q}_s$) and exogenous force ($\vec{\mathcal{F}}_e$) influences on the payload.

Similarly, for the "dirty box" problem, a new input and a new output are defined by

$$\vec{u} = \mathbf{C}^T \vec{f}_m \tag{2.21}$$

$$\vec{y} = \mathbf{C}^T \vec{f}_b \,. \tag{2.22}$$

Then (2.10) can be written as

$$\begin{aligned} \vec{y} = {} & s^2(\mathbf{I}s^2 + \mathbf{\Lambda}s + \frac{1}{\alpha}\mathbf{\Lambda})^{-1}\vec{u} - \mathbf{C}^T\mathbf{M}_q s^2 \vec{q}_s + \\ & s^2(\mathbf{I}s^2 + \alpha s + \tfrac{1}{\alpha}\mathbf{\Lambda})^{-1}\mathbf{C}^T(\mathbf{M}_q s^2 + \mathbf{B}s + \mathbf{K})\vec{q}_s + \\ & [s^2(\mathbf{I}s^2 + \mathbf{\Lambda}s + \tfrac{1}{\alpha}\mathbf{\Lambda})^{-1} - \mathbf{I}]\mathbf{C}^T\mathbf{J}^{-T} {}^{U}_{B}\mathbf{R}^T\vec{\mathcal{F}}_e \;\; . \end{aligned} \tag{2.23}$$

Since $s^2(\mathbf{I}s^2 + \mathbf{\Lambda}s + \frac{1}{\alpha}\mathbf{\Lambda})^{-1}$ is a diagonal transfer function matrix, once again, the dynamics from $\vec{u}$ to $\vec{y}$ are decoupled. SISO LTI compensators from $\vec{u}$ to $\vec{y}$ can be designed to suppress the base acceleration and exogenous force disturbances.

2.3 Decoupling the Pointing Model

Although all the derivations are based on the pointing model given by (1.14), the results of this section can be easily extended to other models in which only part of all six DOFs in the Cartesian space are concerned.

McInroy et al. [25] proposed a decoupling algorithm for the pointing model based on the Jacobian matrix. The decoupling transformation is defined by

$$\vec{f}_m = \mathbf{J} \begin{bmatrix} 1 & 0 \\ 0 & 1 \\ 0 & 0 \\ 0 & 0 \\ 0 & 0 \\ 0 & 0 \end{bmatrix} \vec{u}. \tag{2.24}$$

Substituting (2.24) into (1.14), it is easy to show that the dynamics from $\vec{u}$ to $\vec{\chi}_a$ are decoupled. However, the same three conditions in Section 2.1 must be met in order to make this algorithm apply.

The new decoupling algorithm only requires that $\mathbf{M}_s$, $\mathbf{B}$, and $\mathbf{K}$ be symmetric matrices satisfying $\mathbf{B} = \alpha\mathbf{K}$. First, rewrite (1.14) as

$$\vec{\chi}_a = \begin{bmatrix} 1 & 0 & 0 & 0 & 0 & 0 \\ 0 & 1 & 0 & 0 & 0 & 0 \end{bmatrix} (\mathbf{J}^T\mathbf{M}_p\mathbf{J}s^2 + \mathbf{J}^T\mathbf{B}\mathbf{J}s + \mathbf{J}^T\mathbf{K}\mathbf{J})^{-1}\mathbf{J}^T\vec{f}_m. \tag{2.25}$$

Since $\mathbf{M}_p$ is positive definite, and $\mathbf{J}$ is invertible, $\mathbf{J}^T\mathbf{M}_p\mathbf{J}$ is positive definite. Moreover, $\mathbf{J}^T\mathbf{B}\mathbf{J}$ and $\mathbf{J}^T\mathbf{K}\mathbf{J}$ are symmetric with $\mathbf{J}^T\mathbf{B}\mathbf{J} = \alpha\mathbf{J}^T\mathbf{K}\mathbf{J}$. Thus $\mathbf{J}^T\mathbf{M}_p\mathbf{J}$, $\mathbf{J}^T\mathbf{B}\mathbf{J}$ and

$\mathbf{J}^T\mathbf{K}\mathbf{J}$ can be simultaneously diagonalized by congruence (for the same reason as in Section 2.2.2), i.e., we can find an invertible matrix $\mathbf{C}$ such that

$$\mathbf{J}^T\mathbf{M}_p\mathbf{J} = \mathbf{C}\mathbf{C}^T \tag{2.26}$$

$$\mathbf{J}^T\mathbf{B}\mathbf{J} = \mathbf{C}\mathbf{\Lambda}\mathbf{C}^T \tag{2.27}$$

$$\mathbf{J}^T\mathbf{K}\mathbf{J} = \frac{1}{\alpha}\mathbf{C}\mathbf{\Lambda}\mathbf{C}^T. \tag{2.28}$$

Substituting equations (2.26,2.27,2.28) into (2.25), we get

$$\vec{\chi}_a = \begin{bmatrix} 1 & 0 & 0 & 0 & 0 & 0 \\ 0 & 1 & 0 & 0 & 0 & 0 \end{bmatrix} \mathbf{C}^{-T}(\mathbf{I}s^2 + \mathbf{\Lambda}s + \frac{1}{\alpha}\mathbf{\Lambda})^{-1}\mathbf{C}^{-1}\mathbf{J}^T\vec{f}_m. \tag{2.29}$$

Clearly, $\mathbf{D}(s) = (\mathbf{I}s^2 + \mathbf{\Lambda}s + \frac{1}{\alpha}\mathbf{\Lambda})^{-1}$ is a diagonal transfer function matrix. Let $\mathbf{D}(s) = \text{diag}[d_1(s), \cdots, d_6(s)]$, $\mathbf{C}^{-1} = [\vec{c}_1, \cdots, \vec{c}_6]$, then

$$\vec{\chi}_a = \begin{bmatrix} \vec{c}_1^T \\ \\ \vec{c}_2^T \end{bmatrix} \mathbf{D}(s)\mathbf{C}^{-1}\mathbf{J}^T\vec{f}_m. \tag{2.30}$$

Let $\begin{bmatrix} \vec{c}_1^T \\ \\ \vec{c}_2^T \end{bmatrix}$ be partitioned as $[\mathbf{C}_1\mathbf{C}_2]$ where $\mathbf{C}_1$ is a 2×2 matrix. If $\mathbf{C}_1$ is invertible, we can define

$$\vec{\chi}_a = \mathbf{C}_1\vec{y} \tag{2.31}$$

$$\vec{f}_m = \mathbf{J}^{-T}\mathbf{C}\begin{bmatrix} 1 & 0 \\ 0 & 1 \\ 0 & 0 \\ 0 & 0 \\ 0 & 0 \\ 0 & 0 \end{bmatrix}\vec{u}. \tag{2.32}$$

Substituting it into (2.30) gives

$$\begin{aligned} \vec{y} &= \mathbf{C}_1^{-1}\begin{bmatrix} \mathbf{C}_1 & \mathbf{C}_2 \end{bmatrix}\mathbf{D}(s)\mathbf{C}^{-1}\mathbf{J}^T\mathbf{J}^{-T}\mathbf{C}\begin{bmatrix} 1 & 0 \\ 0 & 1 \\ 0 & 0 \\ 0 & 0 \\ 0 & 0 \\ 0 & 0 \end{bmatrix}\vec{u} \\ &= \begin{bmatrix} d_1(s) & 0 \\ 0 & d_2(s) \end{bmatrix}\vec{u}. \end{aligned} \tag{2.33}$$

It is clear that the dynamics from $\vec{u}$ to $\vec{y}$ are decoupled.

2.4 Experimental Results

The decoupling algorithms have been experimentally verified on one of the UW's mutually orthogonal hexapods. The mechanical parts of the hexapod are all custom machined based on a NASA Jet Propulsion Laboratory design. All six struts are identical. A 200

MHz Gateway 2000 Pentium II computer running the QNX real time operating system sends commands through Computers Boards 16 bit DAC converters to Techron linear current amplifiers. These power BEI voice coil actuators provide base forces ($\vec{f}_b$) measured by PCB quartz force rings mounted on the bottom end of each strut. The payload accelerations along the strut directions ($\ddot{\vec{p}}_u$) are measured by KISTLER-BEAM accelerometers mounted on the top of the spherical joints connecting the payload. The force and acceleration signals are sampled by the control computer's 16 bit analog to digital converters at a rate of 5kHz. Each strut has a maximum stroke of $\pm$ .025 inches.

The performance of the new algorithm in Section 2.2.1 is compared to that obtained using the algorithm in [27]. In [27], a new input and a new output are defined as

$$\vec{u} = \mathbf{J}^T \vec{f}_m \tag{2.34}$$

$$\vec{y} = \mathbf{J}^T \vec{f}_b \tag{2.35}$$

Bode magnitude plots from u_5 (input of channel 5) to $\vec{y}$ (all six channels) are shown in Figure 2.1.

Using the $\mathbf{M}_p$ matrix calculated from the design parameters of the hexapod, a new input and a new output are defined using (2.4) and (2.5). Bode magnitude plots from u_5 to $\vec{y}$ are shown in Figure 2.2.

Finally using the identified joint space mass-inertia matrix (where the identification algorithm used is that discussed in Chapter 3), $\hat{\mathbf{M}}_p$, a new input and a new output are found from (2.4) and (2.5). Bode magnitude plots from u_5 to $\vec{y}$ are shown in Figure 2.3.

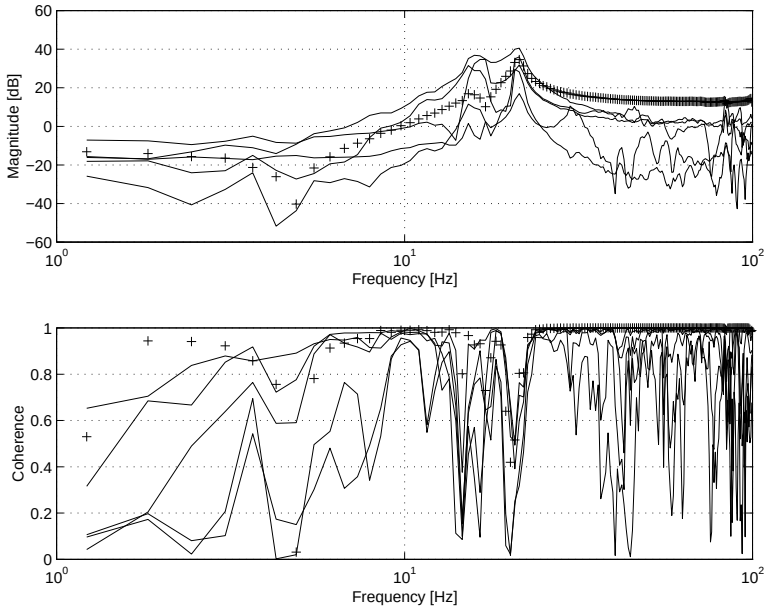

Figure 2.1: Using $\mathbf{J}^T$ as decoupling matrix. The payload's center of mass does not coincide with the center of the cube formed by six orthogonal struts. Bode magnitude plot and coherence from u_5 to $\vec{y}$. y_5 is denoted by "+" signs.

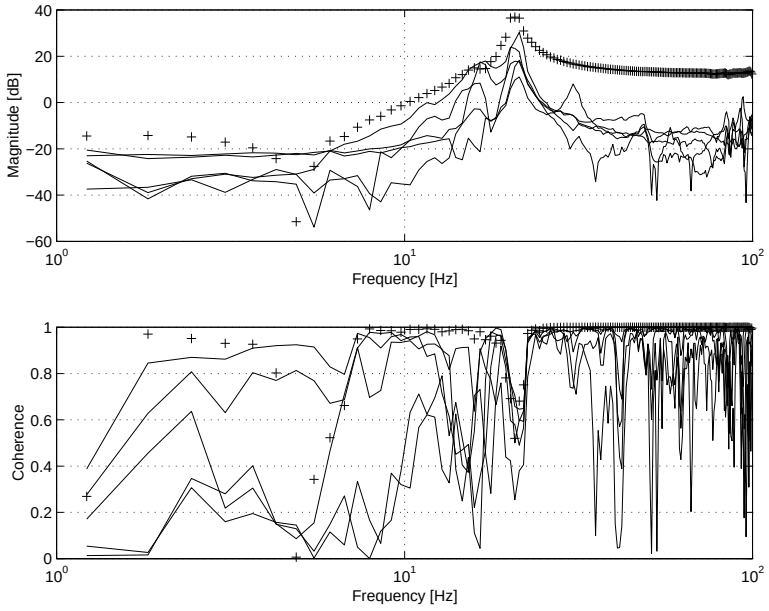

Figure 2.2: Using $\mathbf{V}^T$ as decoupling matrix ($\mathbf{V}^T$ is calculated from $\mathbf{M}_p$). The payload's center of mass does not coincide with the center of the cube formed by six orthogonal struts. Bode magnitude plot and coherence from u_5 to $\vec{y}$. y_5 is denoted by "+" signs.

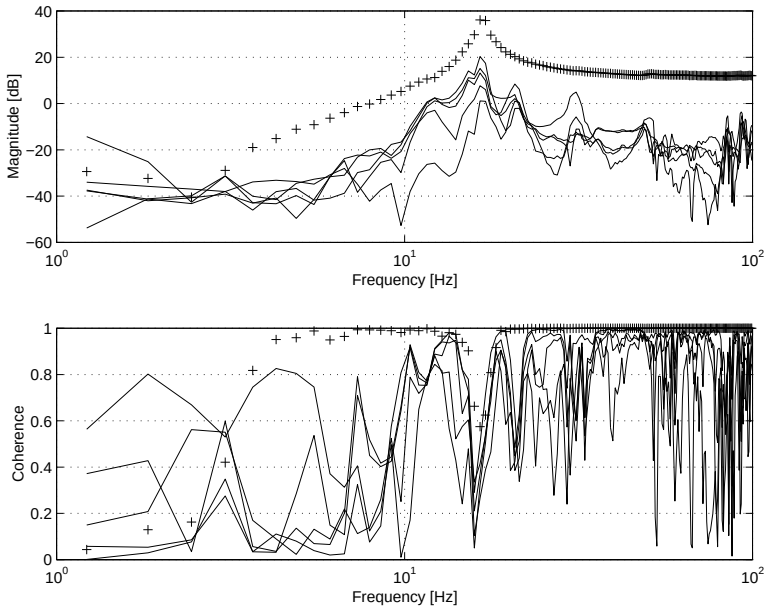

Figure 2.3: Using $\mathbf{V}^T$ as decoupling matrix ($\mathbf{V}^T$ is calculated from $\hat{\mathbf{M}}_p$). The payload's center of mass does not coincide with the center of the cube formed by six orthogonal struts. Bode magnitude plot and coherence from u_5 to $\vec{y}$. y_5 is denoted by "+" signs.

In the experiments, the counterweight placed on the payload is removed. Thus the payload's center of mass doesn't coincide with the center of the cube formed by the orthogonal struts. This explains the results in Figure 2.1. We can see that using decoupling transformations (2.34) and (2.35), there are still strong couplings among all six channels. The input channel (channel 5) is difficult to distinguish from the others. However, using the calculated $\mathbf{M_p}$ matrix and the new decoupling transform (2.4) and (2.5), channel 5 is 3 times (10 dB) stronger (Figure 2.2). When the estimated joint space mass-inertia matrix $\hat{\mathbf{M}}_p$ and the new decoupling transform (2.4) and (2.5) are used, channel 5 is almost 10 times (20dB) stronger across nearly all frequencies (in Figure 2.3). In addition, in all three experiments, the transfer function estimate for channel 5 displays much more coherence than the other channels. Moreover, among

the transfer function estimates for channel 5, the estimated transfer function using the identified decoupling matrix shows the best coherence.

Using the same experimental setup, the decoupling algorithm for the pointing model is also verified. The results using the old method (2.24) are shown in Figure 2.4. As we can see, there are strong couplings between two channels.

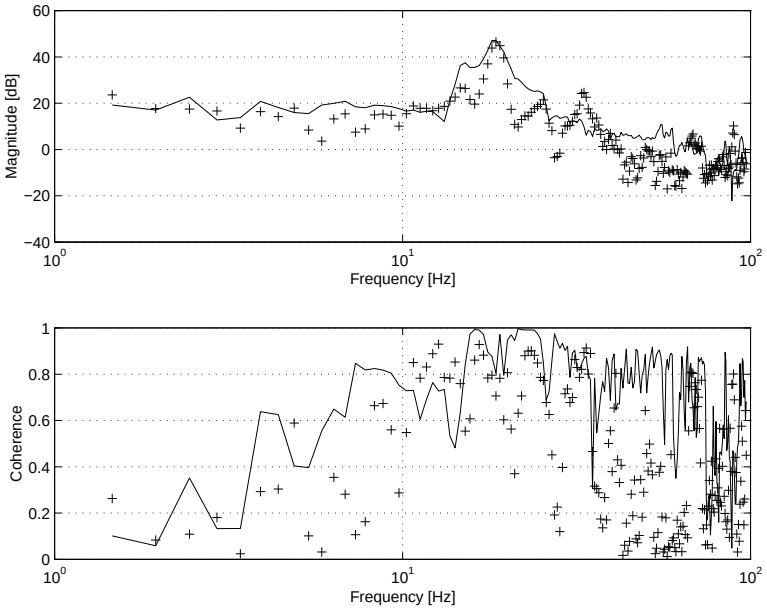

Figure 2.4: Using the first two columns of **J** as decoupling matrix. The payload's center of mass does not coincide with the center of the cube formed by six orthogonal struts. Bode magnitude plot and coherence from u_1 to $\vec{y}$. y_1 is denoted by "+" signs.

The results of the new decoupling algorithms given by (2.31) and (2.32) are shown in Figure 2.5. There is an average of 20dB of difference between two channels in the frequency range $[1, 20]$Hz which is the range that the pointing control system is expected to work in.

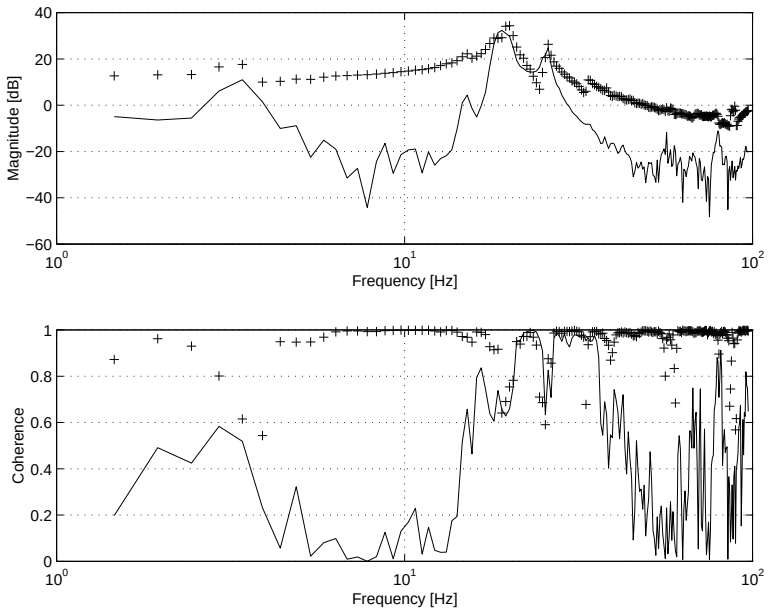

Figure 2.5: Using new decoupling matrix. The payload's center of mass does not coincide with the center of the cube formed by six orthogonal struts. Bode magnitude plot and coherence from u_1 to $\vec{y}$. y_1 is denoted by "+" signs.

Chapter 3

Estimation of Symmetric, Positive Definite Matrices from Imperfect Measurements

In a number of contexts relevant to control problems, including estimation of robot dynamics, covariance, and smart structure mass and stiffness matrices, we need to solve an over-determined set of linear equations $\mathbf{AX} \approx \mathbf{B}$ with the constraint that the matrix $\mathbf{X}$ be symmetric and positive definite. In the classical least squares method the measurements of $\mathbf{A}$ are assumed to be free of error, hence, all errors are confined to $\mathbf{B}$. Thus, the "optimal" solution is given by minimizing the optimization criterion $\|\mathbf{AX} - \mathbf{B}\|_F^2$. However, this assumption is often impractical. Sampling errors, modeling errors, and, sometimes, human errors bring inaccuracies to $\mathbf{A}$. In this chapter, we introduce a different optimization criterion, based on area, which takes the errors in both $\mathbf{A}$ and $\mathbf{B}$ into consideration. Under the condition that the data matrices $\mathbf{A}$ and $\mathbf{B}$ are full rank, which in practice is easy to satisfy, the analytic expression of the global optimizer is derived. A method to handle the case that $\mathbf{A}$ is full rank and $\mathbf{B}$ loses rank is also discussed. Experimental results indicate that the new approach is practical and improves performance of

estimating symmetric and positive definite matrices.

3.1 Related Work

Estimation of symmetric positive definite matrices is required when solving a variety of control problems including robotic control, smart structure control, and intelligent control. In robotics, the mass-inertia matrix of a robotic system is in the symmetric positive definite class, and the accuracy of its estimate directly affects control performance [38][33][6]. Similarly, controlling vibrations and precise positions of "smart" structures often requires estimation of the structure's mass and stiffness matrices [28] [30]; both are symmetric and positive definite. In intelligent control, control decisions are often made based on estimation of a covariance matrix [35][24][17], which is, of course, symmetric and positive definite. Estimation of symmetric positive definite matrices also appears, to a lesser extent, in fields outside control including the educational testing [9] and matrix modification problems [10]. Most of the above examples can be formulated directly or indirectly into finding an optimal solution of a set of linear equations

$$\mathbf{AX} \approx \mathbf{B} \tag{3.1}$$

where $\mathbf{A}, \mathbf{B} \in \mathbb{R}^{m \times n}$ are given, $\mathbf{X} \in \mathbb{P}$ is the fitting matrix, $\mathbb{P}$ is the set of symmetric and positive definite matrices with size $n \times n$. For example, the estimation of the joint space mass-inertia matrix of a flexure jointed hexapod (Stewart Platform) [6] and stiffness matrix directly fit into (3.1). The covariance matrix estimation problem and the matrix modification problem (with symmetric positive definite constraint) can be regarded as

extracting a symmetric positive definite matrix ($\mathbf{C}^*$) from a symmetric but indefinite matrix ($\mathbf{C}$). Thus it can be formulated as solving $\mathbf{CX} \approx \mathbf{I}$ where $\mathbf{X} \in \mathbb{P}$, $\mathbf{I}$ being the identity matrix of size $n \times n$. The "optimal" (under certain criterion) $\mathbf{C}^*$ is given by $\mathbf{C}^* = \mathbf{X}^{-1}$.

There is a rich resource of prior work on this type of problem. Space limitations do not allow us to present a broad survey. Instead we try to emphasize some of the work that is most related to our work. Higham [14] and Brock [3] find an optimal symmetric estimate using the least squares approach (Symmetric Procrustes Problem). Although the positive definite constraint is not considered in their methods, Higham shows that the estimate will be positive definite (semi-definite) if the data matrix $\mathbf{A}^T\mathbf{B} + \mathbf{B}^T\mathbf{A}$ is positive definite (semi-definite). If $\mathbf{A}^T\mathbf{B} + \mathbf{B}^T\mathbf{A}$ is indefinite, then nothing can be concluded about the definiteness of the estimate. Hu [18] presents a least squares based method to handle the positive definite constraint. In his method, the upper and lower bounds for each entry of the fitting matrix must be given explicitly as the constraint. A non-negative scalar is also introduced as a constraint, which measures the degree of positive definiteness. Using the least squares criterion, $\|\mathbf{AX} - \mathbf{B}\|_F^2$, the problem can also be cast as a semi-definite program [41] by specifying lower (and/or upper) bounds of the eigenvalues of $\mathbf{X}$.

Nevertheless, in many applications, there is a question of the suitability of the least squares criterion $\|\mathbf{AX} - \mathbf{B}\|_F^2$. In the classical least squares approach, the measurements $\mathbf{A}$ are supposed to be free of error, hence, all errors are restricted to $\mathbf{B}$. However, this assumption is frequently impractical. Sampling errors, modeling errors, and, some-

times, human errors bring inaccuracies to **A**. For example, in the estimation of a flexure jointed hexapod's joint space mass-inertia matrix [6], **A** and **B** contain the measurements of payload accelerations and base forces, respectively. As a result, sampling and instrument noise appear in both **A** and **B**. Similar phenomena happen in identifying a robot dynamic model [20]. Thus, it is natural for one to expect improved performance by employing a criterion that is capable of describing the errors occurring in both measurement matrices, rather than using the least squares criterion in which only the errors in **B** are considered.

In this chapter, we present a new method of solving an over-determined set of linear equations (3.1) with **X** being symmetric positive definite, and both **A** and **B** containing errors.

3.2 Problem Formulation

A simple example will be more intuitive than a complex one for illustrating and understanding the motivation for the new optimization criterion. So let's consider the following problem with only one variable: estimating a single parameter from a set of over-determined equations

$$\vec{a}x \approx \vec{b}$$

where $\vec{a} = [a_1, a_2, \cdots, a_m]^T$, $\vec{b} = [b_1, b_2, \cdots, b_m]^T \in \mathbb{R}^m$ are known data vectors with $\vec{a}^T\vec{a} > 0$ and $\vec{b}^T\vec{b} > 0$, $x \in \mathbb{R}$ is the variable to be estimated. Using the classical least squares approach, the solution is the minimizer of the optimization criterion $(\vec{b}-\vec{a}x)^T(\vec{b}-$

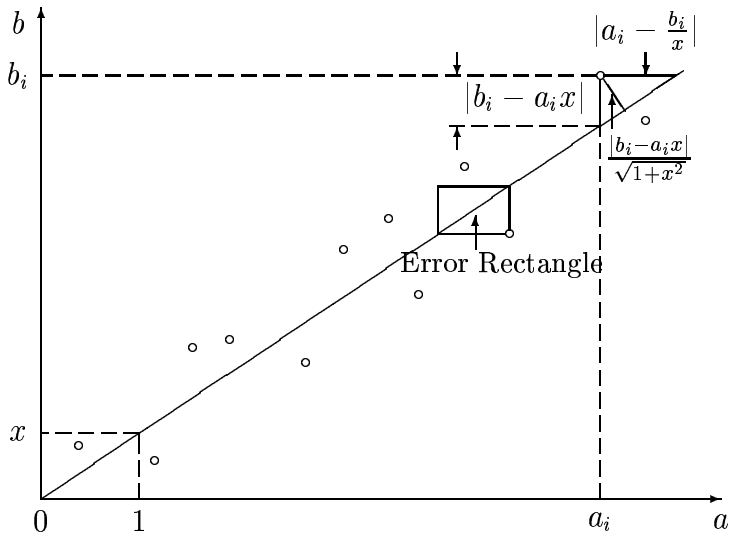

Figure 3.1: Geometric interpretations of one parameter estimation using the least squares, the total least squares, and the new approaches.

$\vec{a}x$) or equivalently $\sum_{i=1}^{m}(b_i - a_i x)^2$. Geometrically, as shown in Figure 3.1, this criterion is the summation of the squared vertical "errors" (the distance from a data point (a_i, b_i) to the fitting line along the direction of the b axis). This criterion is reasonable if the errors only occur in the data vector $\vec{b}$, because we are making predictions based on $\vec{a}$ that is free of error. If the errors are confined to $\vec{a}$, and $\vec{b}$ is free of error, the least squares approach is still appropriate, because we can minimize $(\vec{a} - \frac{\vec{b}}{x})^T(\vec{a} - \frac{\vec{b}}{x})$ or equivalently $\sum_{i=1}^{m}(a_i - \frac{b_i}{x})^2$, which will give the estimate of $\frac{1}{x}$. As shown in Figure 3.1, this time, the least squares solution minimizes the summation of the squared horizontal "errors" (the distance from a data point to the fitting line along the direction of the a axis).

However, in many applications, both $\vec{a}$ and $\vec{b}$ are measurements containing errors. Under this scenario, a more appropriate approach of fitting is the total least squares method [40] (termed orthogonal regression or errors-in-variables regression in the statisti-

cal literature). For the above single parameter estimation problem, the total least squares solution minimizes $\sum_{i=1}^{m} \frac{(b_i - a_i x)^2}{(1+x^2)}$, which, as shown in Figure 3.1, is the summation of the squared minimum "errors" (the minimum distance from a data point to the fitting line). From the properties of the right triangle we can easily derive $\frac{(b_i - a_i x)^2}{(1+x^2)} = \frac{(b_i - a_i x)^2 (a_i - \frac{b_i}{x})^2}{(b_i - a_i x)^2 + (a_i - \frac{b_i}{x})^2}$, i.e., the minimum "error" contains the information of both the vertical "error" and the horizontal "error".

Motivated by the above geometric interpretations of the least squares and the total least squares methods, we introduce a new optimization criterion, the area criterion, which is defined as the summation of the areas of the "error rectangles", i.e., $\sum_{i=1}^{m} |b_i - a_i x||a_i - \frac{b_i}{x}|$. As shown in Figure 3.1, the ith "error rectangle" is constructed by the ith vertical and ith horizontal "errors". Considering the symmetric and positive definite constraints (in this example, it implies $x > 0$), the area criterion can be equivalently written as

$$\begin{aligned} \sum_{i=1}^{m} |b_i - a_i x| \left| a_i - \frac{b_i}{x} \right| &= \sum_{i=1}^{m} (a_i x - b_i) \left(a_i - \frac{b_i}{x} \right) \\ &= (\vec{a} y^2 - \vec{b})^T \left(\vec{a} - \frac{\vec{b}}{y^2} \right) \\ &= \left\| \vec{a} y - \frac{\vec{b}}{y} \right\|_2^2 \end{aligned}$$

where $y \in \mathbb{R}$, $y \neq 0$, $x = yy^T = y^2$. Note that we have transformed the positive constraint on x to the invertible constraint on y.

Now let's consider the original problem given by (3.1). The area criterion is then extended as $\mathrm{Tr}[(\mathbf{AX} - \mathbf{B})^T (\mathbf{A} - \mathbf{BX}^{-1})]$ where $\mathbf{AX} - \mathbf{B}$ represents the errors in $\mathbf{B}$ from the predictions based on $\mathbf{A}$, and $\mathbf{A} - \mathbf{BX}^{-1}$ represents the errors in $\mathbf{A}$ from the

predictions based on $\mathbf{B}$. Using the properties of matrix calculus and the well known fact that $\mathbf{X} = \mathbf{Y}\mathbf{Y}^T$ for any $\mathbf{X} \in \mathbb{P}$, where $\mathbf{Y} \in \mathbb{I}$ and $\mathbb{I}$ is the set of real invertible matrices, the above extended area criterion can be equivalently written as $\|\mathbf{A}\mathbf{Y} - \mathbf{B}\mathbf{Y}^{-T}\|_F^2$. Thus, we can define an optimization problem as follows.

Definition 3.1 *(Symmetric Positive Definite Estimation problem, SPDE) For an over-determined set of m linear equations* $\mathbf{A}\mathbf{X} \approx \mathbf{B}$*, where* $\mathbf{A}, \mathbf{B} \in \mathbb{R}^{m \times n}$ *are given,* $\mathbf{X} \in \mathbb{P}$ *is the fitting matrix, let the area criterion,* $f : \mathbb{I} \to \mathbb{R}$*, be defined as*

$$f(\mathbf{Y}) = \|\mathbf{A}\mathbf{Y} - \mathbf{B}\mathbf{Y}^{-T}\|_F^2 \tag{3.2}$$

with $\|\cdot\|_F$ *being the Frobenius norm of a real matrix. The SPDE problem seeks to minimize the area criterion on* $\mathbb{I}$*. The symmetric positive definite estimate* $\mathbf{X}^*$ *is given by* $\mathbf{X}^* = \mathbf{Y}^*\mathbf{Y}^{*T}$ *where* $\mathbf{Y}^*$ *is a minimizer of (3.2).*

3.3 Finding the Optimizer

To simplify derivations, we introduce two optimization criteria which differ from (3.2) by only a constant.

Lemma 3.2 *Let* $g : \mathbb{I} \to \mathbb{R}$ *and* $h : \mathbb{P} \to \mathbb{R}$ *be defined by*

$$g(\mathbf{Y}) = \mathrm{Tr}(\mathbf{Y}^{\mathrm{T}}\mathbf{P}\mathbf{Y} + \mathbf{Y}^{-1}\mathbf{Q}\mathbf{Y}^{-\mathrm{T}}), \tag{3.3}$$

$$h(\mathbf{X}) = \mathrm{Tr}(\mathbf{P}\mathbf{X} + \mathbf{X}^{-1}\mathbf{Q}) \tag{3.4}$$

where $\mathbf{P} = \mathbf{A}^T\mathbf{A}$ *and* $\mathbf{Q} = \mathbf{B}^T\mathbf{B}$*. Then minimizing* $f(\mathbf{Y})$ *on* $\mathbb{I}$*, minimizing* $g(\mathbf{Y})$ *on* $\mathbb{I}$*,*

and minimizing $h(\mathbf{X})$ *on* $\mathbb{P}$ *are equivalent, i.e.,* $\mathbf{Y}^* \in \mathbb{I}$ *minimizes* $f(\mathbf{Y})$ *if and only if* $\mathbf{Y}^*$ *minimizes* $g(\mathbf{Y})$ *if and only if* $\mathbf{X}^* = \mathbf{Y}^*\mathbf{Y}^{*T} \in \mathbb{P}$ *minimizes* $h(\mathbf{X})$.

Proof: From the identities in matrix calculus, we have

$$f(\mathbf{Y}) = g(\mathbf{Y}) - 2\,\mathrm{Tr}(\mathbf{A}^T\mathbf{B}) = h(\mathbf{X}) - 2\,\mathrm{Tr}(\mathbf{A}^T\mathbf{B}) \tag{3.5}$$

where $\mathbf{X} = \mathbf{Y}\mathbf{Y}^T$. □

In the following two theorems, we assume that $\mathrm{Rank}(\mathbf{A}) = \mathrm{Rank}(\mathbf{B}) = n$, i.e., $\mathbf{P}, \mathbf{Q} \in \mathbb{P}$. This assumption is easy to satisfy in most applications. At the end of this section, we show that with only minor modification the results can be easily extended to the case that $\mathbf{A}$ is full rank and $\mathbf{B}$ loses rank.

Lemma 3.2 implies that it is sufficient to derive the normal equation for one of the optimization criteria ($f(\mathbf{Y})$, $g(\mathbf{Y})$, or $h(\mathbf{X})$). We derive the normal equation for $g(\mathbf{Y})$ as follows.

Theorem 3.3 *Let* $g(\mathbf{Y})$ *be defined by (3.3). If* $\mathbf{Y}^*$ *is a minimizer of* $g(\mathbf{Y})$*, then it satisfies*

$$\mathbf{Y}^*\mathbf{Y}^{*T}\mathbf{P}\mathbf{Y}^*\mathbf{Y}^{*T} = \mathbf{Q}. \tag{3.6}$$

Proof: Let $g' : \mathbb{X} \times \mathbb{X} \to \mathbb{R}$ be defined as

$$g'(\mathbf{Y}, \mathbf{Z}) = \mathrm{Tr}(\mathbf{Y}^T\mathbf{P}\mathbf{Y} + \mathbf{Z}\mathbf{Q}\mathbf{Z}^T)$$

where $\mathbb{X}$ is the set of real $n \times n$ matrices. Then minimizing $g(\mathbf{Y})$ on $\mathbb{I}$ is equivalent to minimizing $g'(\mathbf{Y}, \mathbf{Z})$ on $\mathbb{X} \times \mathbb{X}$ with the constraint $\mathbf{Y}\mathbf{Z} = \mathbf{I}$ where $\mathbf{I} \in \mathbb{R}^{n \times n}$ is the identity matrix.

Let $\mathbf{Y}, \mathbf{Z}, \mathbf{\Psi} \in \mathbb{X}$, $\mathbf{Y} = [\vec{y}_1, \vec{y}_2, \cdots, \vec{y}_n]^T$, and $\mathbf{Z} = [\vec{z}_1, \vec{z}_2, \cdots, \vec{z}_n]$. Let y_{ij}, z_{ij}, and ψ_{ij} be the ijth entries of $\mathbf{Y}$, $\mathbf{Z}$, and $\mathbf{\Psi}$, respectively. The Lagrangian, $L : \mathbb{X} \times \mathbb{X} \times \mathbb{X} \to \mathbb{R}$, associated with the constraint $\mathbf{YZ} = \mathbf{I}$ is defined as

$$L(\mathbf{Y}, \mathbf{Z}, \mathbf{\Psi}) = \mathrm{Tr}[\mathbf{Y}^T\mathbf{P}\mathbf{Y} + \mathbf{Z}\mathbf{Q}\mathbf{Z}^T + \mathbf{\Psi}(\mathbf{YZ} - \mathbf{I})].$$

Setting the partial derivatives of L with respect to y_{ij}, z_{ij}, and ψ_{ij} to 0's for all $1 \leq i, j \leq n$ gives,

$$2\mathbf{Y}^T\mathbf{P} + \mathbf{Z}\mathbf{\Psi} = \mathbf{0}, \tag{3.7}$$

$$2\mathbf{Q}\mathbf{Z}^T + \mathbf{\Psi}\mathbf{Y} = \mathbf{0}, \tag{3.8}$$

$$\mathbf{YZ} = \mathbf{I}. \tag{3.9}$$

Solving (3.7-3.9) for $\mathbf{Y}$ gives (3.6). □

Theorem 3.3 and Lemma 3.2 imply two facts:

1. Any symmetric and positive definite estimate, $\mathbf{X}^*$, of the SPDE problem must satisfy

$$\mathbf{X}^*\mathbf{P}\mathbf{X}^* = \mathbf{Q} \tag{3.10}$$

where $\mathbf{X}^* = \mathbf{Y}^*\mathbf{Y}^{*T}$, $\mathbf{Y}^*$ is a solution of (3.6).

2. Any minimizer for (3.4) must also satisfy (3.10).

However, we still need to show that the solutions (or a solution) of (3.6) minimize(s) (3.3). From Lemma 3.2 and the above facts, this is equivalent to verifying that the solutions (or a solution) of (3.10) minimize(s) (3.4), which is proven in the following theorem.

Theorem 3.4 *The unique minimizer of (3.4), which is the unique solution of (3.10), is given by*

$$\mathbf{X}^* = \mathbf{U_P}\mathbf{\Sigma_P}^{-1}\mathbf{U_{\tilde{Q}}}\mathbf{\Sigma_{\tilde{Q}}}\mathbf{U_{\tilde{Q}}}^T\mathbf{\Sigma_P}^{-1}\mathbf{U_P}^T \tag{3.11}$$

where

$$\mathbf{P} = \mathbf{U_P}\mathbf{\Sigma_P}^2\mathbf{U_P}^T, \tag{3.12}$$

$$\mathbf{\tilde{Q}} = \mathbf{\Sigma_P}\mathbf{U_P}^T\mathbf{Q}\mathbf{U_P}\mathbf{\Sigma_P} = \mathbf{U_{\tilde{Q}}}\mathbf{\Sigma_{\tilde{Q}}}^2\mathbf{U_{\tilde{Q}}}^T \tag{3.13}$$

are the Schur decomposition of $\mathbf{P}$ *and* $\mathbf{\tilde{Q}}$ *respectively, and*

$$\begin{aligned}\mathbf{\Sigma_P} &= \mathrm{diag}[\sqrt{\lambda_{\mathbf{P}}^1}, \sqrt{\lambda_{\mathbf{P}}^2}, \cdots, \sqrt{\lambda_{\mathbf{P}}^n}],\\ \mathbf{\Sigma_{\tilde{Q}}} &= \mathrm{diag}[\sqrt{\lambda_{\tilde{\mathbf{Q}}}^1}, \sqrt{\lambda_{\tilde{\mathbf{Q}}}^1}, \cdots, \sqrt{\lambda_{\tilde{\mathbf{Q}}}^n}]\end{aligned}$$

where $\lambda_{\mathbf{P}}^i$*'s and* $\lambda_{\tilde{\mathbf{Q}}}^j$*'s are eigenvalues of* $\mathbf{P}$ *and* $\mathbf{\tilde{Q}}$*, respectively.*

Proof: Substituting (3.12) into (3.10) gives

$$\mathbf{X}^*\mathbf{U_P}\mathbf{\Sigma_P}\mathbf{U_P}^T\mathbf{U_P}\mathbf{\Sigma_P}\mathbf{U_P}^T\mathbf{X}^* = \mathbf{Q}. \tag{3.14}$$

Left multiplying both sides of (3.14) by $\mathbf{\Sigma_P}\mathbf{U_P}^T$, right multiplying both sides of (3.14) by $\mathbf{U_P}\mathbf{\Sigma_P}$, substituting (3.13) into (3.14), and collecting terms, we have

$$(\mathbf{\Sigma_P}\mathbf{U_P}^T\mathbf{X}^*\mathbf{U_P}\mathbf{\Sigma_P})^2 = (\mathbf{U_{\tilde{Q}}}\mathbf{\Sigma_{\tilde{Q}}}\mathbf{U_{\tilde{Q}}}^T)^2.$$

It is clear that $(\mathbf{U_{\tilde{Q}}}\mathbf{\Sigma_{\tilde{Q}}}\mathbf{U_{\tilde{Q}}}^T)^2 \in \mathbb{P}$, and $\mathbf{X}^* \in \mathbb{P}$ iff $\mathbf{\Sigma_P}\mathbf{U_P}^T\mathbf{X}^*\mathbf{U_P}\mathbf{\Sigma_P} \in \mathbb{P}$. Since a symmetric positive definite matrix has a unique symmetric positive definite square root, we have

$$\mathbf{\Sigma_P}\mathbf{U_P}^T\mathbf{X}^*\mathbf{U_P}\mathbf{\Sigma_P} = \mathbf{U_{\tilde{Q}}}\mathbf{\Sigma_{\tilde{Q}}}\mathbf{U_{\tilde{Q}}}^T. \tag{3.15}$$

Solving (3.15) gives (3.11).

Next we will show that the $\mathbf{X}^*$ given by (3.11) minimizes $h(\mathbf{X})$. Let the Schur decomposition of $\mathbf{X} \in \mathbb{P}$ be

$$\mathbf{X} = \mathbf{U}_\mathbf{X} \mathbf{\Sigma}_\mathbf{X}^2 \mathbf{U}_\mathbf{X}^T \tag{3.16}$$

where $\mathbf{\Sigma}_\mathbf{X} = \text{diag}[\sqrt{\lambda_\mathbf{X}^1}, \sqrt{\lambda_\mathbf{X}^2}, \cdots, \sqrt{\lambda_\mathbf{X}^n}]$ with $\lambda_\mathbf{X}^i$ being the ith eigenvalue of $\mathbf{X}$. Equation (3.13) can be written as

$$\mathbf{Q} = \mathbf{U}_\mathbf{P} \mathbf{\Sigma}_\mathbf{P}^{-1} \mathbf{U}_{\tilde{\mathbf{Q}}} \mathbf{\Sigma}_{\tilde{\mathbf{Q}}} \mathbf{U}_{\tilde{\mathbf{Q}}}^T \mathbf{U}_{\tilde{\mathbf{Q}}} \mathbf{\Sigma}_{\tilde{\mathbf{Q}}} \mathbf{U}_{\tilde{\mathbf{Q}}}^T \mathbf{\Sigma}_\mathbf{P}^{-1} \mathbf{U}_\mathbf{P}^T. \tag{3.17}$$

Substituting equations (3.12,3.16,3.17) into (3.4), we have

$$\begin{aligned}
h(\mathbf{X}) &= Tr(\mathbf{U}_\mathbf{P} \mathbf{\Sigma}_\mathbf{P}^2 \mathbf{U}_\mathbf{P}^T \mathbf{U}_\mathbf{X} \mathbf{\Sigma}_\mathbf{X}^2 \mathbf{U}_\mathbf{X}^T + \mathbf{U}_\mathbf{P} \mathbf{\Sigma}_\mathbf{P}^{-1} \mathbf{U}_{\tilde{\mathbf{Q}}} \mathbf{\Sigma}_{\tilde{\mathbf{Q}}} \mathbf{U}_{\tilde{\mathbf{Q}}}^T \mathbf{U}_{\tilde{\mathbf{Q}}} \mathbf{\Sigma}_{\tilde{\mathbf{Q}}} \mathbf{U}_{\tilde{\mathbf{Q}}}^T \mathbf{\Sigma}_\mathbf{P}^{-1} \mathbf{U}_\mathbf{P}^T \mathbf{U}_\mathbf{X} \mathbf{\Sigma}_\mathbf{X}^{-2} \mathbf{U}_\mathbf{X}^T) \\
&= Tr[(\mathbf{\Sigma}_\mathbf{P} \mathbf{U}_\mathbf{P}^T \mathbf{U}_\mathbf{X} \mathbf{\Sigma}_\mathbf{X})(\mathbf{\Sigma}_\mathbf{X} \mathbf{U}_\mathbf{X}^T \mathbf{U}_\mathbf{P} \mathbf{\Sigma}_\mathbf{P}) + (\mathbf{U}_{\tilde{\mathbf{Q}}} \mathbf{\Sigma}_{\tilde{\mathbf{Q}}} \mathbf{U}_{\tilde{\mathbf{Q}}}^T \mathbf{\Sigma}_\mathbf{P}^{-1} \mathbf{U}_\mathbf{P}^T \mathbf{U}_\mathbf{X} \mathbf{\Sigma}_\mathbf{X}^{-1}) \\
&\quad (\mathbf{\Sigma}_\mathbf{X}^{-1} \mathbf{U}_\mathbf{X}^T \mathbf{U}_\mathbf{P} \mathbf{\Sigma}_\mathbf{P}^{-1} \mathbf{U}_{\tilde{\mathbf{Q}}} \mathbf{\Sigma}_{\tilde{\mathbf{Q}}} \mathbf{U}_{\tilde{\mathbf{Q}}}^T)] \\
&= Tr[(\mathbf{\Sigma}_\mathbf{P} \mathbf{U}_\mathbf{P}^T \mathbf{U}_\mathbf{X} \mathbf{\Sigma}_\mathbf{X} - \mathbf{U}_{\tilde{\mathbf{Q}}} \mathbf{\Sigma}_{\tilde{\mathbf{Q}}} \mathbf{U}_{\tilde{\mathbf{Q}}}^T \mathbf{\Sigma}_\mathbf{P}^{-1} \mathbf{U}_\mathbf{P}^T \mathbf{U}_\mathbf{X} \mathbf{\Sigma}_\mathbf{X}^{-1})(\mathbf{\Sigma}_\mathbf{P} \mathbf{U}_\mathbf{P}^T \mathbf{U}_\mathbf{X} \mathbf{\Sigma}_\mathbf{X} - \\
&\quad \mathbf{U}_{\tilde{\mathbf{Q}}} \mathbf{\Sigma}_{\tilde{\mathbf{Q}}} \mathbf{U}_{\tilde{\mathbf{Q}}}^T \mathbf{\Sigma}_\mathbf{P}^{-1} \mathbf{U}_\mathbf{P}^T \mathbf{U}_\mathbf{X} \mathbf{\Sigma}_\mathbf{X}^{-1})^T + \mathbf{\Sigma}_\mathbf{P} \mathbf{U}_\mathbf{P}^T \mathbf{U}_\mathbf{X} \mathbf{\Sigma}_\mathbf{X} \mathbf{\Sigma}_\mathbf{X}^{-1} \mathbf{U}_\mathbf{X}^T \mathbf{U}_\mathbf{P} \mathbf{\Sigma}_\mathbf{P}^{-1} \mathbf{U}_{\tilde{\mathbf{Q}}} \mathbf{\Sigma}_{\tilde{\mathbf{Q}}} \mathbf{U}_{\tilde{\mathbf{Q}}}^T + \\
&\quad \mathbf{U}_{\tilde{\mathbf{Q}}} \mathbf{\Sigma}_{\tilde{\mathbf{Q}}} \mathbf{U}_{\tilde{\mathbf{Q}}}^T \mathbf{\Sigma}_\mathbf{P}^{-1} \mathbf{U}_\mathbf{P}^T \mathbf{U}_\mathbf{X} \mathbf{\Sigma}_\mathbf{X}^{-1} \mathbf{\Sigma}_\mathbf{X} \mathbf{U}_\mathbf{X}^T \mathbf{U}_\mathbf{P} \mathbf{\Sigma}_\mathbf{P}] \\
&= \|\mathbf{\Sigma}_\mathbf{P} \mathbf{U}_\mathbf{P}^T \mathbf{U}_\mathbf{X} \mathbf{\Sigma}_\mathbf{X} - \mathbf{U}_{\tilde{\mathbf{Q}}} \mathbf{\Sigma}_{\tilde{\mathbf{Q}}} \mathbf{U}_{\tilde{\mathbf{Q}}}^T \mathbf{\Sigma}_\mathbf{P}^{-1} \mathbf{U}_\mathbf{P}^T \mathbf{U}_\mathbf{X} \mathbf{\Sigma}_\mathbf{X}^{-1}\|_F^2 + 2\,\text{Tr}(\mathbf{\Sigma}_{\tilde{\mathbf{Q}}}).
\end{aligned} \tag{3.18}$$

It is clear that $h(\mathbf{X})$ achieves the global minimum when

$$\mathbf{\Sigma}_\mathbf{P} \mathbf{U}_\mathbf{P}^T \mathbf{U}_\mathbf{X} \mathbf{\Sigma}_\mathbf{X} = \mathbf{U}_{\tilde{\mathbf{Q}}} \mathbf{\Sigma}_{\tilde{\mathbf{Q}}} \mathbf{U}_{\tilde{\mathbf{Q}}}^T \mathbf{\Sigma}_\mathbf{P}^{-1} \mathbf{U}_\mathbf{P}^T \mathbf{U}_\mathbf{X} \mathbf{\Sigma}_\mathbf{X}^{-1}, \tag{3.19}$$

and $\mathbf{X}^*$ is the only solution to (3.19). □

Corollary 3.5 *The symmetric positive definite estimate,* $\mathbf{X}^*$*, of the SPDE problem is given by equation (3.11). The minimum of the area criterion,* $f(\mathbf{Y})$*, is* $2\mathrm{Tr}(\mathbf{\Sigma}_{\tilde{\mathbf{Q}}} - \mathbf{A}^{\mathrm{T}}\mathbf{B})$.

Proof: It follows directly from the Definition 3.1 and equations (3.5,3.18). □

Remark 3.6 *Actually, the set of linear equations (3.1) to be solved need not be over-determined. All the above results still hold when* $m = n$ *provided that* $Rank(\mathbf{A}) = Rank(\mathbf{B}) = n$.

Remark 3.7 *Theorem 3.4 says that* $h(\mathbf{X})$ *has a unique minimizer on* $\mathbb{P}$*. But the minimizers of* $f(\mathbf{Y})$ *or* $g(\mathbf{Y})$ *on* $\mathbb{I}$ *are not unique. In fact, it is easy to show that if* $\mathbf{Y}^* \in \mathbb{I}$ *is a minimizer of* $f(\mathbf{Y})$ *or* $g(\mathbf{Y})$ *then* $\mathbf{Y}^*\mathbf{U}$ *is also a minimizer of* $f(\mathbf{Y})$ *and* $g(\mathbf{Y})$ *for any orthonormal matrix* $\mathbf{U}$*. Thus* $f(\mathbf{Y})$ *and* $g(\mathbf{Y})$ *have infinitely many minimizers on* $\mathbb{I}$*. Moreover, all these minimizers are related to the unique minimizer,* $\mathbf{X}^*$*, of* $h(\mathbf{X})$ *on* $\mathbb{P}$ *by* $\mathbf{Y}^*\mathbf{Y}^{*T} = \mathbf{X}^*$*. Consequently, the symmetric positive definite estimate of the SPDE problem is unique.*

In the above discussions the data matrices $\mathbf{A}$ and $\mathbf{B}$ are assumed to be full rank. If either $\mathbf{A}$ or $\mathbf{B}$ lose rank, the method described above can't produce a symmetric positive definite optimizer. However, if $\mathbf{B}$ loses rank and $\mathbf{A}$ remains full rank, i.e., $\mathbf{P} \in \mathbb{P}$ and $\mathbf{Q} \in \overline{\mathbb{P}}$ (the set of symmetric positive semi-definite matrices), we can still find a positive semi-definite optimizer provided that $h(\mathbf{X})$ is optimized on $\overline{\mathbb{P}}_{\mathrm{Rank}(\mathbf{Q})}$ (the set of symmetric positive semi-definite matrices with rank equal to the rank of $\mathbf{Q}$), and $\mathbf{X}^{-1}$ in $h(\mathbf{X})$ is replaced by $\mathbf{X}^{+}$ (Moore-Penrose pseudo-inverse of $\mathbf{X}$). The result is given as follows.

Corollary 3.8 *If* $\mathbf{P} \in \mathbb{P}$, $\mathbf{Q} \in \overline{\mathbb{P}}$, $\mathrm{Rank}(\mathbf{Q}) = \mathrm{r}$, *then the* $\mathbf{X}^* \in \overline{\mathbb{P}}_r$ *given by equation (3.11) minimizes the optimality criterion* $\overline{h}(\mathbf{X}) = \mathrm{Tr}(\mathbf{PX} + \mathbf{X}^+\mathbf{Q})$. *The global minimum of* $\overline{h}(\mathbf{X})$ *on* $\overline{\mathbb{P}}_r$ *equals* $2\mathrm{Tr}(\mathbf{\Sigma}_{\tilde{\mathbf{Q}}})$.

Proof: The proof is similar to that of Theorem 3.4. □

3.4 Numerical Results

In this section, two numerical examples of estimating symmetric positive definite matrices are given. The least squares (LS) estimates [14] and the estimates using the new (SPDE) method are compared.

The first example is the identification of the joint space mass-inertia matrix, $\mathbf{M}_p$, of a University of Wyoming (UW) flexure jointed hexapod [6]. In the vibration isolation control of the flexure jointed hexapod, the performance depends critically on the precision of the decoupling matrix which is calculated from the joint space mass-inertia matrix of the hexapod. Although $\mathbf{M}_p$ can be calculated from the design parameters of the hexapod, it is laborious to do so and can introduce errors due to manufacturing variances and payload changes. Thus a better approach is to estimate $\mathbf{M}_p$ from the measured payload accelerations and base forces.

The relationship between payload accelerations and base forces is described as $\mathbf{AM}_p \approx \mathbf{B}$ [1] where $\mathbf{A}$ contains the payload accelerations, $\mathbf{B}$ contains the base forces, and there are sampling and instrument noise in both $\mathbf{A}$ and $\mathbf{B}$. The matrix data given below

[1] Here we assume the base is kept stationary and there are no exogenous generalized forces exerted on the payload when doing the identification experiment. These constraints can be easily satisfied.

is calculated from the real design parameters of the UW's flexure jointed hexapod.

$$\mathbf{M}_p = \begin{bmatrix} 4.688 & 0.198 & -0.404 & 1.798 & -0.405 & 0.611 \\ 0.198 & 4.688 & 0.611 & -0.405 & 1.798 & -0.404 \\ -0.404 & 0.611 & 4.688 & 0.198 & -0.404 & 1.798 \\ 1.798 & -0.405 & 0.198 & 4.688 & 0.611 & -0.404 \\ -0.405 & 1.798 & -0.404 & 0.611 & 4.688 & 0.198 \\ 0.611 & -0.404 & 1.798 & -0.404 & 0.198 & 4.688 \end{bmatrix}.$$

Six PCB load cells measure force and six Kistler accelerometers measure acceleration to provide the data. For both methods, 100 experiments were performed and the absolute mean and the standard deviation of the estimation errors for 21 independent parameters (since $\mathbf{M}$ is a 6×6 symmetric matrix) are shown in Figure 3.2. Compared with the LS method, the SPDE method provides more precise estimates for all 21 parameters.

In the second numerical example, we are trying to estimate a 2×2 symmetric positive definite matrix, $\mathbf{X}$, from a set of linear equations $(\mathbf{A}+\mathbf{V}_a)\mathbf{X} \approx \mathbf{B}+\mathbf{V}_b$ where $\mathbf{A}+\mathbf{V}_a$ and $\mathbf{B}+\mathbf{V}_b$ are noise-corrupted data matrices,$\mathbf{V}_b$ contains normal distributed noises with 0 mean and standard deviation $\mathrm{STD}\{v_b\} = 1$, $\mathbf{V}_a$ contains normal distributed noises with 0 mean and standard deviation, $\mathrm{STD}\{v_a\}$, varying from 0 to 1.9 in the experiments, $\mathbf{X} = [x_{ij}] = \begin{bmatrix} 3 & 1 \\ 1 & 1 \end{bmatrix}$, $\mathbf{A} = \begin{bmatrix} 5 & -3 & 1 & -1 \\ 2 & 1 & -2 & 1 \end{bmatrix}^T$, $\mathbf{B} = \begin{bmatrix} 17 & -8 & 1 & -2 \\ 7 & -2 & -1 & 0 \end{bmatrix}^T$. At each value of $\mathrm{STD}\{v_a\}$, the absolute mean and the standard deviation of the estimation errors for x_{11}, x_{12}, and x_{22} are calculated for both methods based on 1000 experiments. As shown in Figure 3.3, the SPDE method outperforms the LS method significantly at large values of $\mathrm{STD}\{v_a\}$. This is reasonable because the area criterion includes the

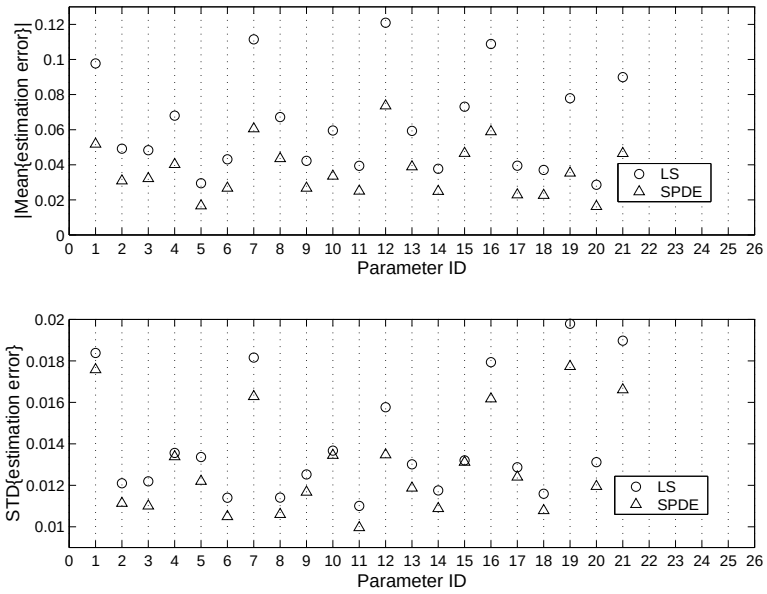

Figure 3.2: Comparison of LS and SPDE methods: absolute mean and standard deviation of the estimation errors of $\mathbf{M}_p$'s entries. Mean{} and STD{} stand for the mean and the standard deviation, respectively.

information of both $\mathbf{V}_b$ and $\mathbf{V}_a$ while the least squares criterion only considers $\mathbf{V}_b$. For the same reason, we can't expect performance improvements when STD$\{v_a\}$ equals 0 or is much smaller than STD$\{v_b\}$, which is also verified by Figure 3.3.

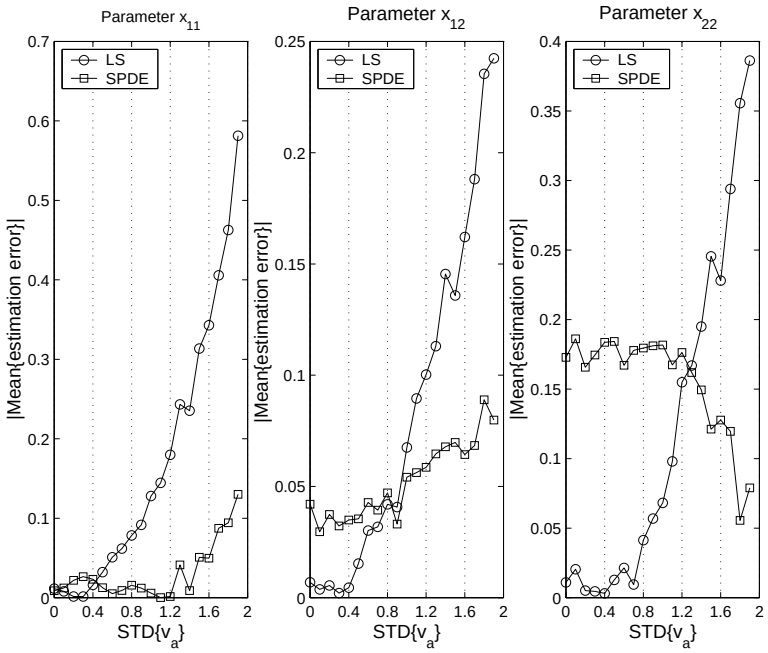

Figure 3.3: Comparison of LS and SPDE methods: absolute mean and standard deviation of the estimation errors of $\mathbf{X}$'s entries. Mean{} and STD{} stand for the mean and the standard deviation, respectively.

Chapter 4

Decoupled Control

In this chapter, we first discuss the relationships between different decoupling algorithms and the disturbance rejection performance of the closed-loop systems. Then the robustness of the system with respect to several perturbation models is briefly presented. Finally, we show that optimal robustness can be achieved by choosing a unitary decoupling matrix.

4.1 Decoupling and Disturbance Rejection

One of the most important goals of feedback control is disturbance rejection. The diagram of a general closed-loop control system is shown in Figure 4.1. $\mathbf{P}(s)$ is the plant transfer function matrix, $\mathbf{K}(s)$ is the controller, $\vec{r}$ is the command signal, $\vec{u}$ is the controller output, $\vec{d_i}$ is the plant input disturbance, $\vec{u}_p$ is the plant input control signal, $\vec{d}$ is the plant output disturbance, $\vec{y}$ is the plant output, $\vec{n}$ is sensor noise. Note that in this chapter we assume that $\mathbf{P}(s)$ is a square transfer function matrix, i.e., the number of inputs of the plant equals the number of outputs of the plant.

Based on Figure 4.1, we make the following definitions,

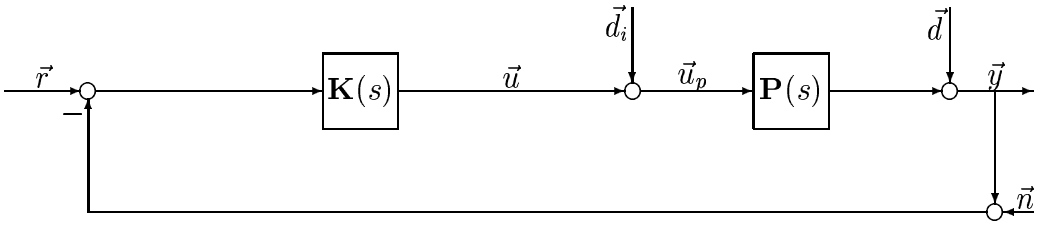

Figure 4.1: A general closed-loop system.

- Input loop transfer matrix

$$\mathbf{L}_i(s) = \mathbf{K}(s)\mathbf{P}(s), \tag{4.1}$$

- Output loop transfer matrix

$$\mathbf{L}_o(s) = \mathbf{P}(s)\mathbf{K}(s), \tag{4.2}$$

- Input sensitivity matrix

$$\mathbf{S}_i(s) = \left[\mathbf{I} + \mathbf{L}_i(s)\right]^{-1}, \tag{4.3}$$

- Output sensitivity matrix

$$\mathbf{S}_o(s) = \left[\mathbf{I} + \mathbf{L}_o(s)\right]^{-1}, \tag{4.4}$$

- Input complementary sensitivity matrix

$$\mathbf{T}_i(s) = \mathbf{I} - \mathbf{S}_i(s) = \mathbf{L}_i(s)\left[\mathbf{I} + \mathbf{L}_i(s)\right]^{-1}, \tag{4.5}$$

- Output complementary sensitivity matrix

$$\mathbf{T}_o(s) = \mathbf{I} - \mathbf{S}_o(s) = \mathbf{L}_o(s)\left[\mathbf{I} + \mathbf{L}_o(s)\right]^{-1}. \tag{4.6}$$

If the closed-loop system given by Figure 4.1 is internally stable [1], then it satisfies

$$\vec{y} = \mathbf{T}_o(s)(\vec{r}-\vec{n}) + \mathbf{S}_o(s)\vec{P}(s)\vec{d_i} + \mathbf{S}_o(s)\vec{d} \tag{4.7}$$

$$\begin{aligned}\vec{u_p} &= \mathbf{K}(s)\mathbf{S}_o(s)(\vec{r}-\vec{n}) - \mathbf{K}(s)\mathbf{S}_o(s)\vec{d} + \mathbf{S}_i(s)\vec{d_i} \\ &= \mathbf{S}_i(s)\mathbf{K}(s)(\vec{r}-\vec{n}) - \mathbf{S}_i(s)\mathbf{K}(s)\vec{d} + \mathbf{S}_i(s)\vec{d_i}.\end{aligned} \tag{4.8}$$

It can be shown [46] that good disturbance rejection at the plant output $\vec{y}$ and the plant input $\vec{u_p}$ for plant input disturbance $\vec{d_i}$ and plant output disturbance $\vec{d}$ require in some frequency range, typically some low-frequency $I_l = (0, \omega_l)$,

$$\underline{\sigma}[\mathbf{L}_o(j\omega)] \gg 1 \tag{4.9}$$

$$\underline{\sigma}[\mathbf{L}_i(j\omega)] \gg 1 \tag{4.10}$$

$$\underline{\sigma}[\mathbf{K}(j\omega)] \gg 1 \tag{4.11}$$

for all $\omega \in I_l$, where $\underline{\sigma}[\mathbf{A}]$ represents the minimum singular value of matrix $\mathbf{A}$. Good sensor noise ($\vec{n}$) rejection at the plant output and the plant input require in some frequency range $I_h = (\omega_h, \infty)$,

$$\overline{\sigma}[\mathbf{L}_o(j\omega)] \ll 1 \tag{4.12}$$

$$\overline{\sigma}[\mathbf{L}_i(j\omega)] \ll 1 \tag{4.13}$$

$$\overline{\sigma}[\mathbf{K}(j\omega)] \leq b \tag{4.14}$$

for all $\omega \in I_h$, where $\overline{\sigma}[\mathbf{A}]$ represents the maximum singular value of matrix $\mathbf{A}$, and b is some positive real number. In addition, $\underline{\sigma}[\mathbf{L}_o(j\omega)]$ and $\overline{\sigma}[\mathbf{L}_o(j\omega)]$ correspond to distur-

[1] Internal stability [46] is a basic requirement for a practical feedback system. It guarantees that all signals in a system are bounded if the input signals, at all locations, are bounded.

bance rejection performance at the plant output, $\underline{\sigma}[\mathbf{L}_i(j\omega)]$ and $\overline{\sigma}[\mathbf{L}_i(j\omega)]$ correspond to disturbance rejection performance at the plant input.

For a single-input single-output (SISO) plant, $\mathbf{P}(s)$ is a scalar system. It is clear that $\mathbf{L}_o(s) = \mathbf{P}(s)\mathbf{K}(s) = \mathbf{K}(s)\mathbf{P}(s) = \mathbf{L}_i(s)$. Thus good disturbance rejection at plant input implies good disturbance rejection at plant output, and vice versa. For multiple-input multiple-output (MIMO) plants, however, $\mathbf{P}(s)$ and $\mathbf{K}(s)$ in general are not commutable in multiplication. Thus, in general, $\underline{\sigma}[\mathbf{L}_o(j\omega)] \neq \underline{\sigma}[\mathbf{L}_i(j\omega)]$ and $\overline{\sigma}[\mathbf{L}_o(j\omega)] \neq \overline{\sigma}[\mathbf{L}_i(j\omega)]$. As a result, good disturbance rejection at plant output (input) doesn't imply good disturbance rejection at plant input (output). The following theorem gives a class of plants that are symmetric in disturbance rejection performance.

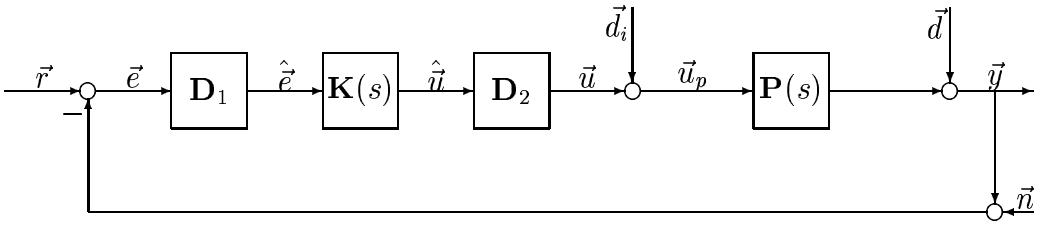

Figure 4.2: A general decoupled control system.

Theorem 4.1 *Consider the closed-loop system given by Figure 4.2. Let* $\mathbf{K}(s)$ *be a diagonal transfer function matrix. If there exists invertible matrices* $\mathbf{D}_1$, $\mathbf{D}_2 \in \mathbb{C}^{n\times n}$ *such that* $\mathbf{D}_1\mathbf{P}(s)\mathbf{D}_2 = \mathbf{\Lambda}(s)$ *is diagonal and* $\mathbf{D}_1\mathbf{D}_2 = \mathbf{D}$ *is diagonal, then the disturbance rejection performance of the closed-loop system at the plant output* $\vec{y}$ *is the same as that at the plant input* $\vec{u}_p$ *for plant input disturbance* $\vec{d}_i$*, plant output disturbance* $\vec{d}$*, and sensor noise* $\vec{n}$*.*

Proof: In Figure 4.2, the controller, $\mathbf{K}'(s)$, of the closed-loop system is defined as

$$\mathbf{K}'(s) = \mathbf{D}_2\mathbf{K}(s)\mathbf{D}_1. \tag{4.15}$$

Thus from (4.1) and (4.2), the input and output loop transfer matrices are

$$\mathbf{L}_i(s) = \mathbf{K}'(s)\mathbf{P}(s) = \mathbf{D}_2\mathbf{K}(s)\mathbf{D}_1\mathbf{P}(s), \tag{4.16}$$

$$\mathbf{L}_o(s) = \mathbf{P}(s)\mathbf{K}'(s) = \mathbf{P}(s)\mathbf{D}_2\mathbf{K}(s)\mathbf{D}_1. \tag{4.17}$$

It is sufficient to show that $\mathbf{L}_o(s) = \mathbf{L}_i(s)$ which are derived as follows

$$\begin{aligned} \mathbf{D}_1\mathbf{L}_i(s)\mathbf{D}_2 &= \mathbf{D}_1\mathbf{D}_2\mathbf{K}(s)\mathbf{D}_1\mathbf{P}(s)\mathbf{D}_2 \\ &= \mathbf{D}\mathbf{K}(s)\mathbf{\Lambda}(s), \end{aligned} \tag{4.18}$$

$$\begin{aligned} \mathbf{D}_1\mathbf{L}_o(s)\mathbf{D}_2 &= \mathbf{D}_1\mathbf{P}(s)\mathbf{D}_2\mathbf{K}(s)\mathbf{D}_1\mathbf{D}_2 \\ &= \mathbf{\Lambda}(s)\mathbf{K}(s)\mathbf{D}. \end{aligned} \tag{4.19}$$

It is clear that $\mathbf{L}_o(s) = \mathbf{L}_i(s)$ because $\mathbf{D}$, $\mathbf{K}(s)$, and $\mathbf{\Lambda}(s)$ are diagonal. □

4.2 Decoupling and Robustness

In most control systems, the controller is designed based on the model of the plant. The quality of the model depends on how well its response matches that of the real plant. However, for almost all practical systems, no single fixed model can respond exactly the same as the true plant. One way to mitigate this discrepancy is to use a set of models to describe a given plant. Consequently, it is desirable that the controller could do its job for all models in the model set, i.e. the closed-loop system is robust.

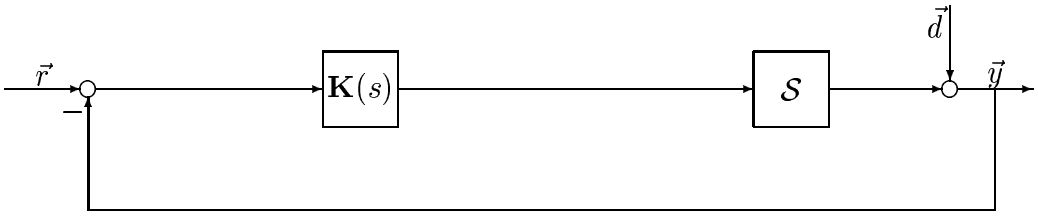

Figure 4.3: A general closed-loop system with model perturbation.

Consider the closed-loop system in Figure 4.3. $\mathcal{S}$ is an uncertainty model set. $\mathbf{P}(s) \in \mathcal{S}$ is the nominal design model. $\mathbf{K}(s)$ is the controller. We define

- Nominal Stability: $\mathbf{K}(s)$ internally stabilizes $\mathbf{P}(s)$.
- Robust Stability: $\mathbf{K}(s)$ internally stabilizes every plant in $\mathcal{S}$.

Different types of uncertainty can be characterized by different perturbed model sets. Here we focus on the following four commonly used uncertainty models sets

$$\mathcal{S}_1 = \left\{ [\mathbf{I} + \mathbf{W}_1(s)\mathbf{\Delta}(s)\mathbf{W}_2(s)]\,\mathbf{P}(s) : \mathbf{\Delta} \in \mathcal{R}H_\infty, \|\mathbf{\Delta}\|_\infty < \frac{1}{\gamma}, \gamma > 0 \right\}, \quad (4.20)$$

$$\mathcal{S}_2 = \left\{ \mathbf{P}(s)\,[\mathbf{I} + \mathbf{W}_1(s)\mathbf{\Delta}(s)\mathbf{W}_2(s)] : \mathbf{\Delta} \in \mathcal{R}H_\infty, \|\mathbf{\Delta}\|_\infty < \frac{1}{\gamma}, \gamma > 0 \right\}, \quad (4.21)$$

$$\mathcal{S}_3 = \left\{ [\mathbf{I} + \mathbf{W}_1(s)\mathbf{\Delta}(s)\mathbf{W}_2(s)]^{-1}\,\mathbf{P}(s) : \mathbf{\Delta} \in \mathcal{R}H_\infty, \|\mathbf{\Delta}\|_\infty < \frac{1}{\gamma}, \gamma > 0 \right\}, \quad (4.22)$$

$$\mathcal{S}_4 = \left\{ \mathbf{P}(s)\,[\mathbf{I} + \mathbf{W}_1(s)\mathbf{\Delta}(s)\mathbf{W}_2(s)]^{-1} : \mathbf{\Delta} \in \mathcal{R}H_\infty, \|\mathbf{\Delta}\|_\infty < \frac{1}{\gamma}, \gamma > 0 \right\} \quad (4.23)$$

where $\mathcal{R}H_\infty$ is the set of all proper real rational stable transfer function matrices, $\mathbf{W}_1(s)$ and $\mathbf{W}_2(s) \in \mathcal{R}H_\infty$ are weighting matrices. It is important to note that

- $\mathcal{S}_1$ represents output sensor errors, high frequency unmodeled dynamics, and right-half plane (rhp) zeros,

- $\mathcal{S}_2$ represents input actuator errors, high frequency unmodeled dynamics, and rhp zeros,
- $\mathcal{S}_3$ represents low frequency parameter errors and rhp poles,
- $\mathcal{S}_4$ represents low frequency parameter errors and rhp poles.

From the Small Gain Theorem [46], the robust stability tests for $\mathcal{S}_1$-$\mathcal{S}_4$ are derived as

$$\|\mathbf{W}_2(s)\mathbf{T}_o(s)\mathbf{W}_1(s)\|_\infty \leq \gamma \tag{4.24}$$

$$\|\mathbf{W}_2(s)\mathbf{T}_i(s)\mathbf{W}_1(s)\|_\infty \leq \gamma \tag{4.25}$$

$$\|\mathbf{W}_2(s)\mathbf{S}_o(s)\mathbf{W}_1(s)\|_\infty \leq \gamma \tag{4.26}$$

$$\|\mathbf{W}_2(s)\mathbf{S}_i(s)\mathbf{W}_1(s)\|_\infty \leq \gamma. \tag{4.27}$$

For SISO plants, $\mathbf{T}_i(s) = \mathbf{T}_o(s)$, and $\mathbf{S}_i(s) = \mathbf{S}_o(s)$. Thus the closed-loop system has robust stability with respect to $\mathcal{S}_1$ ($\mathcal{S}_3$) iff it has robust stability with respect to $\mathcal{S}_2$ ($\mathcal{S}_4$). But for general MIMO plants, this nice property doesn't hold. However, there are a class of MIMO plants for which the closed-loop system can be designed to be symmetric in robust stability.

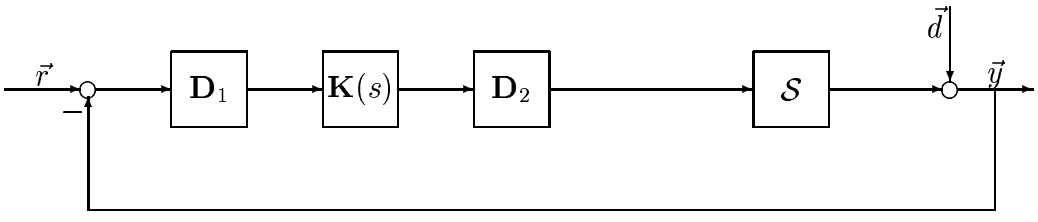

Figure 4.4: A general decoupled control system with model perturbation.

Theorem 4.2 *Consider the closed-loop system given by Figure 4.4. Let* $\mathbf{K}(s)$ *be a diagonal transfer function matrix. If there exists invertible matrices* $\mathbf{D}_1$, $\mathbf{D}_2 \in \mathbb{C}^{n\times n}$ *such that* $\mathbf{D}_1\mathbf{P}(s)\mathbf{D}_2 = \mathbf{\Lambda}(s)$ *is diagonal and* $\mathbf{D}_1\mathbf{D}_2 = \mathbf{D}$ *is diagonal, then*

- *the closed-loop system is robustly stable for* $\mathcal{S} \cap (\mathcal{S}_1 \cup \mathcal{S}_2)$ *if and only if it is robustly stable for* $\mathcal{S} \cap \mathcal{S}_1$ *or* $\mathcal{S} \cap \mathcal{S}_2$
- *the closed-loop system is robustly stable for* $\mathcal{S} \cap (\mathcal{S}_3 \cup \mathcal{S}_4)$ *if and only if it is robustly stable for* $\mathcal{S} \cap \mathcal{S}_3$ *or* $\mathcal{S} \cap \mathcal{S}_4$

Proof: In the proof of Theorem 4.1, we have shown that $\mathbf{L}_o(s) = \mathbf{L}_i(s)$. Together with (4.3), (4.4), (4.5), and (4.6), we have

$$\mathbf{T}_o(s) = \mathbf{T}_i(s) \tag{4.28}$$

$$\mathbf{S}_o(s) = \mathbf{S}_i(s) \tag{4.29}$$

As a result,

$$\|\mathbf{W}_2(s)\mathbf{T}_o(s)\mathbf{W}_1(s)\|_\infty \le \gamma \iff \|\mathbf{W}_2(s)\mathbf{T}_i(s)\mathbf{W}_1(s)\|_\infty \le \gamma \tag{4.30}$$

$$\|\mathbf{W}_2(s)\mathbf{S}_o(s)\mathbf{W}_1(s)\|_\infty \le \gamma \iff \|\mathbf{W}_2(s)\mathbf{S}_i(s)\mathbf{W}_1(s)\|_\infty \le \gamma. \tag{4.31}$$

This completes the proof. □

4.3 Unitary Decoupling and Optimal Robust Controller

The Small Gain Theorem tells us that the smaller the value of $\|\mathbf{W}_2\mathbf{T}_o(s)\mathbf{W}_1(s)\|_\infty$ the larger the permissible $\|\mathbf{\Delta}\|_\infty$ for uncertainty model set $\mathcal{S}_1$, i.e., the more robust the system is to $\mathcal{S}_1$.

For the closed-loop system shown in Figure 4.3, we call $\lambda_i[\mathbf{P}(s)\mathbf{K}(s)], i = 1, \cdots, n$ the open-loop characteristic functions which are the eigenfunctions of $\mathbf{P}(s)\mathbf{K}(s)$. $\lambda_i(s)$'s describe the dynamic performance of the closed-loop system, and are therefore important design parameters. Zhang [45] proved that for the closed-loop system shown in Figure 4.3, among all the controllers that satisfy the given open-loop characteristic functions, $\|\mathbf{W}_2\mathbf{T}_o(s)\mathbf{W}_1(s)\|_\infty$ achieves minimum if $\mathbf{P}(s)\mathbf{K}(s)$ is normal [2] where $\mathcal{S} = \mathcal{S}_1$, $\mathbf{W}_1(s)$ is diagonal, $\mathbf{W}_2(s) = \mathbf{I}$.

Based on the above property, the following theorem describes the relationship between decoupling transformations and the optimal robust controller.

Theorem 4.3 *Consider the closed-loop system given by Figure 4.3 where* $\mathcal{S} = \mathcal{S}_1$. $\lambda_i(s), i = 1, \cdots, n$ *are given open-loop characteristic functions. Define the set of feasible controllers as* $\mathcal{K} = \{\mathbf{K}(s) : \lambda_i[\mathbf{P}(s)\mathbf{K}(s)] = \lambda_i(s), i = 1, \cdots, n\}$. *If there exists a controller* $\mathbf{K}'(s) = \mathbf{D}_2\mathbf{K}_d(s)\mathbf{D}_1 \in \mathcal{K}$, *where* $\mathbf{D}_1$, $\mathbf{D}_2 \in \mathbb{C}^{n\times n}$ *are invertible matrices,* $\mathbf{K}_d(s) \in \mathcal{R}H_\infty$ *is diagonal, such that* $\mathbf{D}_1\mathbf{P}(s)\mathbf{D}_2 = \mathbf{\Lambda}(s)$ *is diagonal,* $\mathbf{D}_1 = \mathbf{D}_2^{-1} = \mathbf{D}_2^H$,

[2] A matrix $\mathbf{A}$ is normal if and only if $\mathbf{A}^H\mathbf{A} = \mathbf{A}\mathbf{A}^H$, where H denotes the conjugate transpose.

then

$$\min_{\mathbf{K}(s)\in\mathcal{K}} \|\mathbf{W}_1(s)\mathbf{P}(s)\mathbf{K}(s)\left[\mathbf{I}+\mathbf{P}(s)\mathbf{K}(s)\right]^{-1}\|_\infty = \|\mathbf{W}_1(s)\mathbf{P}(s)\mathbf{K}'(s)\left[\mathbf{I}+\mathbf{P}(s)\mathbf{K}'(s)\right]^{-1}\|_\infty \tag{4.32}$$

where the weighting matrix $\mathbf{W}_1(s) \in \mathcal{R}H_\infty$ *is diagonal.*

Proof: It is sufficient to show that $\mathbf{P}(s)\mathbf{D}_2\mathbf{K}_d(s)\mathbf{D}_1$ is normal.

Since

$$\mathbf{D}_1\mathbf{D}_1^H = \mathbf{I} \tag{4.33}$$

$$\begin{aligned}\mathbf{D}_1\mathbf{P}(s)\mathbf{D}_2\mathbf{K}_d(s)\mathbf{D}_1\mathbf{D}_2 &= \mathbf{D}_1\mathbf{P}(s)\mathbf{D}_2\mathbf{K}_d(s)\mathbf{D}_1\mathbf{D}_1^H \\ &= \mathbf{\Lambda}(s)\mathbf{K}_d(s)\end{aligned} \tag{4.34}$$

$\mathbf{P}(s)\mathbf{D}_2\mathbf{K}_d(s)\mathbf{D}_1$ is unitarily diagonalized, thus is normal. □

Remark 4.4 *Theorem 4.3 tells us that if we can find a unitary constant transformation matrix to decouple the plant, and use SISO techniques to design the compensator (*$\mathbf{D}_1\mathbf{P}(s)\mathbf{D}_2$ *and* $\mathbf{K}_d(s)$ *are diagonal) so that the performance is satisfied (in terms of open-loop characteristic functions), then the closed-loop system also has the best robustness with respect to uncertainty model set* $\mathcal{S}_1$ *(and from Theorem 4.2,* $\mathcal{S}_2$*) compared with all the other controllers that generate the same open-loop characteristic functions.*

Chapter 5

Optimal, Fault-Tolerant Velocity and Static Force Mapping for Prioritized Manipulation

From a kinematic viewpoint, a manipulator is redundant if the number of joints is greater than the number of degrees of freedom (DOFs) of its end-effector. This extra freedom offers many advantages over conventional nonredundant manipulators including kinematic singularity avoidance, fault tolerance, workspace obstacle avoidance, energy (joint torque) minimization, joint limit avoidance, and dexterity improvement [2], [4],[5],[15],[19], [23],[22],[34], [44], etc.

In all the references listed above and most of the other previous work on redundant manipulators, the redundancy comes from the joint space (redundant joints). However, in many applications the redundancy can also occur in Cartesian space (operational space) [31]. For example, in welding, rotations about the welding rod may be irrelevant. Similarly, when pointing a camera at distant objects, orientation is more important than position. Thus the DOFs related to orientation (for welding) or position (for pointing a camera) can be viewed as redundant in the sense that they can be sacrificed for some par-

ticular reasons such as avoiding obstacles in the workspace, optimizing certain kinematic performance indices, or tolerating actuator failures, etc. We call these manipulations prioritized manipulations. Since prioritized manipulations may be performed either by kinematically redundant or "ordinary" manipulators, the theory developed here is applicable to both. A manipulator performing prioritized manipulation tasks is called a prioritized manipulator. The end-effector's DOFs during a prioritized manipulation can be divided into major DOFs (MDOFs), which are more important in performing a task, and secondary DOFs (SDOFs), which are less important in performing a task. Explicit treatment of these redundancies is important because different motions along the SDOFs may require significantly larger joint velocity or torque. In general, both MDOFs and SDOFs can be a mixture of position and orientation.

Motivated by the optimal fault-tolerant pointing application of a Stewart platform ([21],[25]), this work focuses on the optimal fault-tolerant velocity and static force mapping for prioritized manipulations. The main goal is to find velocity and static force mappings that optimize different performance indices, satisfy certain constraints, and can handle actuator failures. Two kinds of common actuator failures (position failure and torque failure) are considered. The position failure acts as if the actuator is locked. The torque failure occurs when the actuator can't provide any torque actively. The problem is solved in two steps: constructing the differential kinematics and static force model (with or without actuator failures) followed by finding the optimal mappings for the given differential kinematics and static force model.

The remainder of this chapter is organized as follows. In Section 5.1, we first summa-

rize the differential kinematics and static force model of a prioritized manipulation based on Wen and Wilfinger's work ([43],[42]). Then we develop a reconfiguration method to treat the position and torque failures. Section 5.2 derives the optimal velocity and static force mappings based on several performance indices. Section 5.3 uses a simple example to illustrate the techniques of Section 5.1 and 5.2.

5.1 Differential Kinematics and Static Force Model

A prioritized manipulation can be performed by a serial robot, a parallel robot, or in a more general sense a constrained rigid multibody system (including a multi-finger hand, multiple cooperative robots, and Stewart platform). Any of these manipulators may also be kinematically redundant. In Section 5.1.1 the differential kinematics and static force model for serial robots and general constrained rigid multibody systems are summarized based on [7], [43], and [42]. In case of actuator failures, reconfiguration methods are discussed in Section 5.1.2. To be consistent with [43] and [42], in this section, we use the following terminology and notation:

- Spatial (general) force at a given frame is an $m \times 1$ vector $\begin{bmatrix} torque \\ force \end{bmatrix}$.
- Spatial (Cartesian) velocity at a given frame is an $m \times 1$ vector $\begin{bmatrix} angular\ velocity \\ linear\ velocity \end{bmatrix}$.
- For a given matrix $\mathbf{G}$, $\widetilde{\mathbf{G}}$ denotes the transpose of the annihilator of $\mathbf{G}^T$ ($\mathbf{G}\widetilde{\mathbf{G}} = \mathbf{0}$).

5.1.1 Nominal Model

Consider serial manipulators and general constrained rigid multibody systems without any actuator failures. Let $\vec{\theta}$ denote the generalized coordinate, $\vec{\theta}_a$ denote the angles of active joints, $\vec{\theta}_p$ denote the angles of passive joints, and $\vec{\tau}$ represent the torque exerted by active joints. For serial manipulators all joints are active joints, i.e. $\vec{\theta} = \vec{\theta}_a$. In case of general constrained rigid multibody systems, the joint angles are partitioned as

$$\vec{\theta} = \begin{bmatrix} \vec{\theta}_a \\ \vec{\theta}_p \end{bmatrix}. \tag{5.1}$$

The differential kinematics and static force model of a serial manipulator [7] are given by

$$\vec{v} = \mathbf{J}(\vec{\theta})\dot{\vec{\theta}}_a \tag{5.2}$$

$$\vec{\tau} = \mathbf{J}(\vec{\theta})^T \vec{f} \tag{5.3}$$

where $\vec{v} \in \mathbb{R}^m$ is the spatial velocity of the end-effector, $\vec{f} \in \mathbb{R}^m$ is the spatial force (the force that the manipulator exerts at the end-effector), $\dot{\vec{\theta}}_a \in \mathbb{R}^n$ is the active joint velocity, $\mathbf{J}(\vec{\theta}) \in \mathbb{R}^{m \times n}$ is the Jacobian matrix . If $\mathbf{J}$ loses row rank, the manipulator is in a singular configuration. This means that there is some direction or subspace in Cartesian space along which it is impossible to move the end-effector no matter what joint rates are selected. In the same direction (or subspace), the end-effector cannot actively exert static forces as desired. That is, $\vec{f}$ could be increased or decreased in some directions, which define the null space of $\mathbf{J}^T$, $\mathcal{N}(\mathbf{J}^T)$, with no effect on the value calculated for $\vec{\tau}$.

When the priority of the DOFs of the end-effector is considered, $\vec{v}$ and $\vec{f}$ can be ordered such that

$$\vec{v} = \begin{bmatrix} \vec{v}_m \\ \vec{v}_s \end{bmatrix} \tag{5.4}$$

$$\vec{f} = \begin{bmatrix} \vec{f}_m \\ \vec{f}_s \end{bmatrix} \tag{5.5}$$

with $\vec{v}_m \in \mathbb{R}^{m_1}$ ($\vec{v}_s \in \mathbb{R}^{m_2}$) denoting the end-effector velocity in the directions or subspace of MDOFs (SDOFs), $\vec{f}_m \in \mathbb{R}^{m_1}$ ($\vec{f}_s \in \mathbb{R}^{m_2}$) denoting the end-effector force in the directions (or subspace) of MDOFs (SDOFs), and $m_1 + m_2 = m$. Rearranging (5.2) and (5.3), we have

$$\begin{bmatrix} \vec{v}_m \\ \vec{v}_s \end{bmatrix} = \begin{bmatrix} \mathbf{J}_m \\ \mathbf{J}_s \end{bmatrix} \dot{\vec{\theta}}_a \tag{5.6}$$

$$\vec{\tau} = \begin{bmatrix} \mathbf{J}_m^T & \mathbf{J}_s^T \end{bmatrix} \begin{bmatrix} \vec{f}_m \\ \vec{f}_s \end{bmatrix} \tag{5.7}$$

where $\mathbf{J}_m \in \mathbb{R}^{m_1 \times n}$, $\mathbf{J}_s \in \mathbb{R}^{m_2 \times n}$. A prioritized serial manipulator is in a singular configuration if $\mathbf{J}_m$ loses row rank since MDOFs are what we really care about.

For a general kinematically constrained rigid multibody system, the differential kinematics model becomes [43]

$$\vec{v} = \mathbf{J}_T(\vec{\theta})\dot{\vec{\theta}} \tag{5.8}$$

with constraints

$$\mathbf{J}_C(\vec{\theta})\dot{\vec{\theta}} = \vec{0} \tag{5.9}$$

where $\vec{\theta}$ is given by (5.1). The static force model follows from the principle of virtual work:

$$\begin{bmatrix} \vec{\tau} \\ \vec{0} \end{bmatrix} = \mathbf{J}_T^T \vec{f} + \mathbf{J}_C^T \vec{f}_C. \tag{5.10}$$

Here $\vec{\tau}$ is the torque applied by active joints, $\vec{f}_C$ is the "internal force"-the force that enforces the constraint (5.9). Note that the passive joints can't apply any torque actively.

In order to find a direct relationship between $\vec{v}$ and $\dot{\vec{\theta}}_a$ ($\vec{\tau}$ and $\vec{f}$), we partition $\mathbf{J}_T$ and $\mathbf{J}_C$ according to the dimension of $\vec{\theta}_a$ and $\vec{\theta}_p$:

$$\mathbf{J}_T = \begin{bmatrix} \mathbf{J}_{T_a} & \mathbf{J}_{T_p} \end{bmatrix} \tag{5.11}$$

$$\mathbf{J}_C = \begin{bmatrix} \mathbf{J}_{C_a} & \mathbf{J}_{C_p} \end{bmatrix}. \tag{5.12}$$

With some matrix operations, we get

$$\vec{v} = \mathbf{J}\dot{\vec{\theta}}_a + \mathbf{J}_{T_p}\widetilde{\mathbf{J}}_{C_p}\vec{\xi} \tag{5.13}$$

$$\vec{\tau} = \mathbf{J}^T\vec{f} + \mathbf{J}_{C_a}^T\widetilde{\mathbf{J}_{C_p}^T}\vec{\eta} \tag{5.14}$$

where $\mathbf{J} \in \mathbb{R}^{m\times n}$ is the manipulability Jacobian defined as

$$\mathbf{J} = \mathbf{J}_{T_a} - \mathbf{J}_{T_p}\mathbf{J}_{C_p}^{+}\mathbf{J}_{C_a}, \tag{5.15}$$

$\vec{\xi}$ and $\vec{\eta}$ are arbitrary. Unlike serial manipulators, there are two kinds of singularities:

- Unmanipulable singularity corresponds to configurations at which $\mathbf{J}$ in (5.13) and (5.14) loses row rank. This is the same as the singularity for serial manipulators.
- Unstable singularity corresponds to configurations at which $\mathbf{J}_{T_p}\widetilde{\mathbf{J}}_{C_p} \neq \mathbf{0}$. Physically, an unstable singularity means that the end-effector can move even when all active joints are locked.

In (5.14), $\widetilde{\mathbf{J}_{C_p}^T \vec{\eta}}$ is called the irresolvable internal force (or free internal force) which belongs to $\mathcal{N}(\mathbf{J}_{C_p}^T)$. A more detailed treatment of the concept of velocity and force manipulability can be found in [43] and [42].

If the priority of the end-effector's DOFs is taken into account, we can order $\vec{v}$ and $\vec{f}$ in the same way as that in (5.4) and (5.5). Thus (5.13) and (5.14) can be rearranged as

$$\begin{bmatrix} \vec{v}_m \\ \vec{v}_s \end{bmatrix} = \begin{bmatrix} \mathbf{J}_m \\ \mathbf{J}_s \end{bmatrix} \dot{\vec{\theta}}_a + \mathbf{J}_{T_p} \widetilde{\mathbf{J}}_{C_p} \vec{\xi} \tag{5.16}$$

$$\vec{\tau} = \begin{bmatrix} \mathbf{J}_m^T & \mathbf{J}_s^T \end{bmatrix} \begin{bmatrix} \vec{f}_m \\ \vec{f}_s \end{bmatrix} + \mathbf{J}_{C_a}^T \widetilde{\mathbf{J}_{C_p}^T \vec{\eta}} \tag{5.17}$$

where $\mathbf{J}_m \in \mathbb{R}^{m_1 \times n}$, $\mathbf{J}_s \in \mathbb{R}^{m_2 \times n}$. Similar to the singularity of prioritized serial manipulators, a prioritized constrained rigid multibody system is in an unmanipulable singular configuration if $\mathbf{J}_m$ loses row rank.

5.1.2 Actuator Failures

A common failure for a robotic manipulator is due to actuators [29]. Examples include motor winding failure, servo controller power failure, bearing failure, gearbox failure, brake failure, etc. Most of the actuator failures can be characterized as either position failure or torque failure. The former acts as if the actuator is locked, i.e. the joint can't change its angle or length. The latter occurs when the actuator can't actively exert any torque, i.e. the joint can only move passively. Many previous works, including [25] and [34], focus on the position failure. In this section, we introduce a reconfiguration method

which can handle the position failure and torque failure as well.

Position Failure

Physically, a joint can't change its angle or length when position failure happens to the actuator. This can be mathematically interpreted as

$$\dot{\theta}_i = 0 \tag{5.18}$$

for some $i \in \{1, \cdots, n\}$. Suppose q position failures occur. Without loss of generality, we assume that failures happen in the first q active joints. This can always be done by arranging $\vec{\theta}_a$ and the corresponding columns of $\mathbf{J}$ (for serial robots) or $\mathbf{J}_T$ and $\mathbf{J}_C$ (for constrained rigid multibody systems). If a passive joint locks, then the analysis is similar so it is excluded for brevity.

Let $\hat{\vec{\theta}}_a = [\theta_{q+1}, \cdots, \theta_n]^T$, $\hat{\vec{\tau}} = [\tau_{q+1}, \cdots, \tau_n]^T$ consisting of angles and torques of active joints without position failures. Considering q constraints in the form of (5.18) with $i = 1, \cdots, q$, the kinematics and static force model for a prioritized serial manipulator, (5.6) and (5.7), can be written as

$$\begin{bmatrix} \vec{v}_m \\ \vec{v}_s \end{bmatrix} = \begin{bmatrix} \hat{\mathbf{J}}_m \\ \hat{\mathbf{J}}_s \end{bmatrix} \dot{\hat{\vec{\theta}}}_a \tag{5.19}$$

$$\hat{\vec{\tau}} = \begin{bmatrix} \hat{\mathbf{J}}_m^T & \hat{\mathbf{J}}_s^T \end{bmatrix} \begin{bmatrix} \vec{f}_m \\ \vec{f}_s \end{bmatrix} \tag{5.20}$$

where $\hat{\mathbf{J}}_m \in \mathbb{R}^{m_1 \times (n-q)}$ is composed of the last $n-q$ columns of $\mathbf{J}_m$ defined in (5.6), $\hat{\mathbf{J}}_s \in \mathbb{R}^{m_2 \times (n-q)}$ is composed of the last $n-q$ columns of $\mathbf{J}_s$ defined in (5.6). Singularity occurs when $\hat{\mathbf{J}}_m$ loses row rank.

Similarly, for a prioritized constrained rigid multibody system with position failure in the first q active joints, we define $\hat{\mathbf{J}}_{T_a}$ and $\hat{\mathbf{J}}_{C_a}$ to be the last $n-q$ columns of $\mathbf{J}_{T_a}$ and $\mathbf{J}_{C_a}$ respectively. It is straightforward to show that

$$\hat{\mathbf{J}} = \hat{\mathbf{J}}_{T_a} - \mathbf{J}_{T_p}\mathbf{J}_{C_p}^{\dagger}\hat{\mathbf{J}}_{C_a} \tag{5.21}$$

consisting of the last $n-q$ columns of $\mathbf{J}$ given by (5.15). The differential kinematics and static force model described by (5.16) and (5.17) can be written as

$$\begin{bmatrix} \vec{v}_m \\ \vec{v}_s \end{bmatrix} = \begin{bmatrix} \hat{\mathbf{J}}_m \\ \hat{\mathbf{J}}_s \end{bmatrix} \dot{\vec{\theta}}_a + \mathbf{J}_{T_p}\widetilde{\mathbf{J}}_{C_p}\vec{\xi} \tag{5.22}$$

$$\vec{\tau} = \begin{bmatrix} \hat{\mathbf{J}}_m^T & \hat{\mathbf{J}}_s^T \end{bmatrix} \begin{bmatrix} \vec{f}_m \\ \vec{f}_s \end{bmatrix} + \hat{\mathbf{J}}_{C_a}^T \widetilde{\mathbf{J}_{C_p}^T}\vec{\eta} \tag{5.23}$$

where $\hat{\mathbf{J}}_m \in \mathbb{R}^{m_1 \times (n-q)}$ consists of the last $n-q$ columns of $\mathbf{J}_m$ defined in (5.16), $\hat{\mathbf{J}}_s \in \mathbb{R}^{m_2 \times (n-q)}$ consists of the last $n-q$ columns of $\mathbf{J}_s$ defined in (5.16). The system is in an unmanipulable singular configuration if $\hat{\mathbf{J}}_m$ loses row rank. Unstable singularity occurs if $\mathbf{J}_{T_p}\widetilde{\mathbf{J}}_{C_p} \neq \mathbf{0}$.

Torque Failure

When torque failure happens to an actuator, the actuator can't exert any torque actively, which implies that the corresponding active joint can't move actively. Note that this doesn't mean that the joint can't move. In fact, an active joint with torque failure can move freely but passively. Thus an active joint with torque failure becomes a passive joint.

Without loss of generality, we suppose that torque failures occur to the first q active joints. This means

$$\tau_i = 0,\ i = 1, \cdots, q. \tag{5.24}$$

For serial manipulators, (5.7) together with (5.24) imply that $\vec{f} \in \{\vec{J}_1, \cdots, \vec{J}_q\}^{\perp}$ where $\vec{J}_i$ is the ith column of $\begin{bmatrix} \mathbf{J}_m \\ \\ \mathbf{J}_s \end{bmatrix}$ in (5.6). Then clearly there exist task frame spatial forces (in span$\{\vec{\mathrm{J}}_1, \cdots, \vec{\mathrm{J}}_{\mathrm{q}}\}$) that can't be balanced by active torques alone. The same situation occurs when a constrained rigid multibody system is in an unstable singular configuration. Thus serial manipulators can't resist any torque failures.

Next, we consider a constrained rigid multibody system with torque failures in the first q active joints. As mentioned above, this is equivalent to changing the first q active joints to passive joints. So we define $\hat{\vec{\theta}}_a = [\theta_{q+1}, \cdots, \theta_n]^T$, $\hat{\vec{\tau}} = [\tau_{q+1}, \cdots, \tau_n]^T$ consisting of angles and torque of active joints without torque failures, $\hat{\vec{\theta}}_p = \left[\theta_1, \cdots, \theta_q, \vec{\theta}_p^T\right]^T$ to be the angles of passive joints. Then we partition $\mathbf{J}_T$ and $\mathbf{J}_C$ according to the dimension of $\vec{\theta}_a$ and $\vec{\theta}_p$:

$$\mathbf{J}_T = \begin{bmatrix} \hat{\mathbf{J}}_{T_a} & \hat{\mathbf{J}}_{T_p} \end{bmatrix} \tag{5.25}$$

$$\mathbf{J}_C = \begin{bmatrix} \hat{\mathbf{J}}_{C_a} & \hat{\mathbf{J}}_{C_p} \end{bmatrix} \tag{5.26}$$

where $\hat{\mathbf{J}}_{T_a}$ consists of the last $n-q$ columns of $\mathbf{J}_{T_a}$, $\hat{\mathbf{J}}_{C_a}$ consists of the last $n-q$ columns of $\mathbf{J}_{C_a}$, $\hat{\mathbf{J}}_{T_p} = \left[\vec{J}_{T_{p1}}, \cdots, \vec{J}_{T_{pq}}, \mathbf{J}_{T_p}\right]$, $\hat{\mathbf{J}}_{C_p} = \left[\vec{J}_{C_{p1}}, \cdots, \vec{J}_{C_{pq}}, \mathbf{J}_{C_p}\right]$, $\vec{J}_{T_{pi}}$ and $\vec{J}_{C_{pi}}$ are the ith column of $\mathbf{J}_{T_p}$ and $\mathbf{J}_{C_p}$ respectively. Thus we can derive the differential kinematics and static force model by replacing $\vec{\theta}_a$, $\mathbf{J}_{T_a}$, $\mathbf{J}_{T_p}$, $\mathbf{J}_{C_a}$, $\mathbf{J}_{C_p}^{\dagger}$, $\widetilde{\mathbf{J}}_{C_p}$, and $\widetilde{\mathbf{J}_{C_p}^T}$ in (5.15,5.16,5.17)

with $\hat{\vec{\theta}}_a$, $\hat{\mathbf{J}}_{T_a}$, $\hat{\mathbf{J}}_{T_p}$, $\hat{\mathbf{J}}_{C_a}$, $\hat{\mathbf{J}}^{\dagger}_{C_p}$, $\widetilde{\hat{\mathbf{J}}_{C_p}}$, and $\widetilde{\hat{\mathbf{J}}^{T}_{C_p}}$ respectively. Finally, unmanipulable singularities and unstable singularities can be analyzed following the same approach as that given in Section 5.1.2. Unlike serial manipulators, constrained rigid multibody systems can tolerate torque failures if $\hat{\mathbf{J}}_{T_p}\widetilde{\hat{\mathbf{J}}_{C_p}} = \mathbf{0}$.

If position failures occur in some joints, while torque failures simultaneously occur in others, then the manipulation can be analyzed by applying both of the above techniques serially.

5.2 Optimal Velocity and Static Force Mapping

For a kinematically redundant manipulator, there are infinite joint velocities that give the same end-effector velocity. Utilizing this property, many different performance indices can be optimized by adding terms in $\mathcal{N}(\mathbf{J})$ to the joint velocities [4],[15],[22], [31]. For prioritized manipulation, the redundancy occurs in Cartesian space. Similarly, this extra freedom can also be used in optimizing certain kinematic performance indices.

Section 5.2.1 converts the trajectory planning problem for prioritized manipulation into an optimization problem in $\mathcal{N}(\mathbf{J})$. Analytical solutions to the problem are derived. Section 5.2.2 finds a velocity mapping with minimum condition number for general redundant manipulators.

5.2.1 Trajectory Planning for Prioritized Manipulation

In this section, we assume that the system is not at a singular position, i.e.:

- For serial manipulators, $\mathbf{J}_m$ has full row-rank.

- For general constrained rigid multibody systems, $\mathbf{J}_m$ has full row-rank and $\mathbf{J}_{T_p}\widetilde{\mathbf{J}}_{C_p} = \mathbf{0}$. In addition, there are no irresolvable internal forces, i.e. $\mathcal{N}(\mathbf{J}_{C_p}^T) = \{\vec{0}\}$.

Thus the differential kinematics and static force model for serial manipulators and general constrained rigid multibody systems can be uniformly written as (5.6) and (5.7). If there are joints failures then the models are reconfigured using the methods in Section 5.1.2.

Let the desired trajectory be given in terms of Cartesian space position $\vec{\chi}_d = \begin{bmatrix} \vec{\chi}_{dm} \\ \vec{\chi}_{ds} \end{bmatrix}$ where $\vec{\chi}_{dm}$ and $\vec{\chi}_{ds}$ correspond to the desired MDOF position and SDOF position, respectively. Let $\vec{\chi} = \begin{bmatrix} \vec{\chi}_m \\ \vec{\chi}_s \end{bmatrix}$ be the actual position of the end-effector(s) with $\vec{\chi}_m$ and $\vec{\chi}_s$ representing MDOF position and SDOF position, respectively. $\delta\vec{\chi} = \begin{bmatrix} \delta\vec{\chi}_m \\ \delta\vec{\chi}_s \end{bmatrix} = \vec{\chi}_d - \vec{\chi}$ is the error between the desired position and the actual position where $\delta\vec{\chi}_m$ is the position error in MDOF, $\delta\vec{\chi}_s$ is the position error in SDOF. $\delta\vec{\chi}$ can be assumed small if the control system does its job. Thus we can rewrite the differential kinematics model (5.6) as

$$\begin{bmatrix} \delta\vec{\chi}_m \\ \delta\vec{\chi}_s \end{bmatrix} = \begin{bmatrix} \mathbf{J}_m \\ \mathbf{J}_s \end{bmatrix} \delta\vec{\theta}_a. \tag{5.27}$$

where $\delta\vec{\theta}_a$ is a small displacement in joint space.

For a given $\delta\vec{\theta}_a$, the Cartesian space displacement of the end-effector(s) is determined by equation 5.27. However, in many applications, only the Cartesian space tra-

jectory is specified, i.e., we need to compute $\delta\vec{\theta}_a$ which can generate the given $\delta\vec{\chi}$. If $\mathbf{J}$ is invertible, the solution is given by $\delta\vec{\theta}_a = \mathbf{J}^{-1}\delta\vec{\chi}$. If $\mathbf{J}$ is not invertible, then $\delta\vec{\theta}_a = \mathbf{J}^{+}\delta\vec{\chi}$ is the minimum length joint space displacement that will produce a Cartesian space displacement closest to, in the least squares sense, the given $\delta\vec{\chi}$.

However, for prioritized manipulations, we don't really need to find a solution which minimizes the difference across all DOFs since MDOFs are more important than SDOFs. In fact, by sacrificing the motions in SDOFs, we can further minimize the difference in MDOFs. Moreover, additional constraints can also be satisfied to achieve joint limits avoidance, workspace obstacle avoidance, and energy minimization, etc. For these reasons, we formulate an optimization problem as follows

Problem 5.1 *Consider the differential kinematics model (5.27). Given desired Cartesian space displacement* $\delta\vec{\chi} = \begin{bmatrix} \delta\vec{\chi}_m \\ \delta\vec{\chi}_s \end{bmatrix} \in \mathbb{R}^m$ *and desired joint space displacement* $\delta\vec{\theta}_d$*, find an actual joint space displacement* $\delta\vec{\theta}_a \in \mathbb{R}^n$ *such that*

$$\delta\vec{\chi}_m = \mathbf{J}_m\delta\vec{\theta}_a, \tag{5.28}$$

and

$$\|\mathbf{W}_1(\delta\vec{\theta}_a - \delta\vec{\theta}_d)\|_2^2 + \|\mathbf{W}_2(\mathbf{J}_s\delta\vec{\theta}_a - \delta\vec{\chi}_s)\|_2^2 \tag{5.29}$$

is minimized. $\mathbf{W}_1 \in \mathbb{R}^{n\times n}$ *and* $\mathbf{W}_2 \in \mathbb{R}^{m_2\times m_2}$ *are weighting matrices.*

Remark 5.2 *In Problem 5.1, we try to find a joint space displacement which will produce the desired MDOF motion. At the same time, the performance criterion, given by (5.29), is minimized. Two terms are included in (5.29).* $\|\mathbf{W}_1(\delta\vec{\theta}_a - \delta\vec{\theta}_d)\|_2^2$ *denotes the*

magnitude of the joint space error where $\delta\vec{\theta}_d$ can be specified for joint limits avoidance or energy minimization, etc. The error in SDOF motion is measured by $\|\mathbf{W}_2(\mathbf{J}_s\delta\vec{\theta}_a - \delta\vec{\chi}_s)\|_2^2$ where $\delta\vec{\chi}_s$ may be specified for workspace obstacle avoidance or dexterity improvement, etc. Note that in general $\delta\vec{\theta}_a$ and $\delta\vec{\chi}$ have elements with different physical units. Adding terms with different units gives a physically meaningless sum. The weighting matrices are used to avoid this kind of inconsistent operation. Methods of finding appropriate weighting matrices can be found in [8].

Depending on the weighting matrices, Problem 5.1 is solved by the following theorems.

Theorem 5.3 *If $\mathbf{W}_1$ and $\mathbf{W}_2$ are nonsingular weighting matrices, the unique solution for Problem 5.1 is*

$$\begin{aligned}\delta\vec{\theta}_a &= \left\{ \mathbf{J}_m^+ - \widetilde{\mathbf{J}}_m \begin{bmatrix} \mathbf{W}_1\widetilde{\mathbf{J}}_m \\ \mathbf{W}_2\mathbf{J}_s\widetilde{\mathbf{J}}_m \end{bmatrix}^+ \begin{bmatrix} \mathbf{W}_1\mathbf{J}_m^+ \\ \mathbf{W}_2\mathbf{J}_s\mathbf{J}_m^+ \end{bmatrix} \right\} \delta\vec{\chi}_m + \\ &\quad \widetilde{\mathbf{J}}_m \begin{bmatrix} \mathbf{W}_1\widetilde{\mathbf{J}}_m \\ \mathbf{W}_2\mathbf{J}_s\widetilde{\mathbf{J}}_m \end{bmatrix}^+ \begin{bmatrix} \mathbf{W}_1 & \mathbf{0} \\ \mathbf{0} & \mathbf{W}_2 \end{bmatrix} \begin{bmatrix} \delta\vec{\theta}_d \\ \delta\vec{\chi}_s \end{bmatrix}. \end{aligned} \tag{5.30}$$

Proof: Given $\delta\vec{\chi}_m \in \mathbb{R}^{m_2}$, all solutions of (5.28) are given by

$$\delta\vec{\theta}_a = \mathbf{J}_m^+\delta\vec{\chi}_m + \widetilde{\mathbf{J}}_m\vec{\zeta} \tag{5.31}$$

where $\vec{\zeta} \in \mathbb{R}^{n-m_1}$ is arbitrary. Thus we have

$$\begin{bmatrix} \mathbf{W}_1(\delta\vec{\theta}_a - \delta\vec{\theta}_d) \\ \mathbf{W}_2(\mathbf{J}_s\delta\vec{\theta}_a - \delta\vec{\chi}_s) \end{bmatrix} = \begin{bmatrix} \mathbf{W}_1\mathbf{J}_m^+ \\ \mathbf{W}_2\mathbf{J}_s\mathbf{J}_m^+ \end{bmatrix} \delta\vec{\chi}_m + \begin{bmatrix} \mathbf{W}_1\widetilde{\mathbf{J}}_m \\ \mathbf{W}_2\mathbf{J}_s\widetilde{\mathbf{J}}_m \end{bmatrix} \vec{\zeta} - \begin{bmatrix} \mathbf{W}_1 & \mathbf{0} \\ \mathbf{0} & \mathbf{W}_2 \end{bmatrix} \begin{bmatrix} \delta\vec{\theta}_d \\ \delta\vec{\chi}_s \end{bmatrix}. \tag{5.32}$$

It is clear that

$$\|\mathbf{W}_1(\delta\vec{\theta}_a - \delta\vec{\theta}_d)\|_2^2 + \|\mathbf{W}_2(\mathbf{J}_s\delta\vec{\theta}_a - \delta\vec{\chi}_s)\|_2^2 = \left\| \begin{bmatrix} \mathbf{W}_1(\delta\vec{\theta}_a - \delta\vec{\theta}_d) \\ \mathbf{W}_2(\mathbf{J}_s\delta\vec{\theta}_a - \delta\vec{\chi}_s) \end{bmatrix} \right\|_2^2. \tag{5.33}$$

Since $\begin{bmatrix} \mathbf{W}_1\widetilde{\mathbf{J}}_m \\ \mathbf{W}_2\mathbf{J}_s\widetilde{\mathbf{J}}_m \end{bmatrix}$ has full column-rank, $\|\mathbf{W}_1(\delta\vec{\theta}_a - \delta\vec{\theta}_d)\|_2^2 + \|\mathbf{W}_2(\mathbf{J}_s\delta\vec{\theta}_a - \delta\vec{\chi}_s)\|_2^2$ is minimized if and only if

$$\vec{\zeta} = -\begin{bmatrix} \mathbf{W}_1\widetilde{\mathbf{J}}_m \\ \mathbf{W}_2\mathbf{J}_s\widetilde{\mathbf{J}}_m \end{bmatrix}^+ \left\{ \begin{bmatrix} \mathbf{W}_1\mathbf{J}_m^+ \\ \mathbf{W}_2\mathbf{J}_s\mathbf{J}_m^+ \end{bmatrix} \delta\vec{\chi}_m - \begin{bmatrix} \mathbf{W}_1 & \mathbf{0} \\ \mathbf{0} & \mathbf{W}_2 \end{bmatrix} \begin{bmatrix} \delta\vec{\theta}_d \\ \delta\vec{\chi}_s \end{bmatrix} \right\}. \tag{5.34}$$

Substituting (5.34) into (5.31) gives (5.30). □

Theorem 5.4 *If* $\mathbf{W}_1$ *is invertible,* $\mathbf{W}_2 = \mathbf{0}$*, then the unique solution for Problem 5.1 is*

$$\delta\vec{\theta}_a = \left[\mathbf{J}_m^+ - \widetilde{\mathbf{J}}_m(\mathbf{W}_1\widetilde{\mathbf{J}}_m)^+\mathbf{W}_1\mathbf{J}_m^+\right]\delta\vec{\chi}_m + \widetilde{\mathbf{J}}_m(\mathbf{W}_1\widetilde{\mathbf{J}}_m)^+\mathbf{W}_1\delta\vec{\theta}_d. \tag{5.35}$$

Proof: From (5.31) we have

$$\mathbf{W}_1(\delta\vec{\theta}_a - \delta\vec{\theta}_d) = \mathbf{W}_1\mathbf{J}_m^+\delta\vec{\chi}_m + \mathbf{W}_1\widetilde{\mathbf{J}}_m\vec{\zeta} - \mathbf{W}_1\delta\vec{\theta}_d. \tag{5.36}$$

Since $\mathbf{W}_1\widetilde{\mathbf{J}}_m$ has full column-rank, $\|\mathbf{W}_1(\delta\vec{\theta}_a - \delta\vec{\theta}_d)\|_2^2$ is minimized if and only if

$$\vec{\zeta} = -(\mathbf{W}_1\widetilde{\mathbf{J}}_m)^+\left[\mathbf{W}_1\mathbf{J}_m^+\delta\vec{\chi}_m - \mathbf{W}_1\delta\vec{\theta}_d\right]. \tag{5.37}$$

Substituting (5.37) into (5.31) we get (5.35). □

Theorem 5.5 *If* $\mathbf{W}_1 = \mathbf{0}$*,* $\mathbf{W}_2$ *is invertible, then the minimum norm solution for Problem 5.1 is*

$$\delta\vec{\theta}_a = \left[\mathbf{I} - \widetilde{\mathbf{J}}_m\widetilde{\mathbf{A}}(\widetilde{\mathbf{J}}_m\widetilde{\mathbf{A}})^+\right]\left[(\mathbf{J}_m^+ - \widetilde{\mathbf{J}}_m\mathbf{A}^+\mathbf{B})\delta\vec{\chi}_m + \widetilde{\mathbf{J}}_m\mathbf{A}^+\mathbf{W}_2\delta\vec{\chi}_s\right] \tag{5.38}$$

where

$$\mathbf{A} = \mathbf{W}_2\mathbf{J}_s\widetilde{\mathbf{J}}_m \tag{5.39}$$

$$\mathbf{B} = \mathbf{W}_2\mathbf{J}_s\mathbf{J}_m^+. \tag{5.40}$$

Proof: From (5.31) we have

$$\mathbf{W}_2(\mathbf{J}_s\delta\vec{\theta}_a - \delta\vec{\chi}_s) = \mathbf{B}\delta\vec{\chi}_m + \mathbf{A}\vec{\zeta} - \mathbf{W}_2\delta\vec{\chi}_s. \tag{5.41}$$

It is clear that $\|\mathbf{W}_2(\mathbf{J}_s\delta\vec{\theta}_a - \delta\vec{\chi}_s)\|_2^2$ is minimized if and only if

$$\vec{\zeta} = -\mathbf{A}^+\left[\mathbf{B}\delta\vec{\chi}_m - \mathbf{W}_2\delta\vec{\chi}_s\right] + \widetilde{\mathbf{A}}\vec{\varsigma} \tag{5.42}$$

where $\vec{\varsigma}$ is arbitrary. Substituting (5.42) into (5.31) yields

$$\delta\vec{\theta}_a = (\mathbf{J}_m^+ - \widetilde{\mathbf{J}}_m\mathbf{A}^+\mathbf{B})\delta\vec{\chi}_m + \widetilde{\mathbf{J}}_m\widetilde{\mathbf{A}}\vec{\varsigma} + \widetilde{\mathbf{J}}_m\mathbf{A}^+\mathbf{W}_2\delta\vec{\chi}_s, \tag{5.43}$$

which tells that $\|\delta\vec{\theta}_a\|_2^2$ is minimized if and only if

$$\vec{\varsigma} = -(\widetilde{\mathbf{J}}_m\widetilde{\mathbf{A}})^+\left[(\mathbf{J}_m^+ - \widetilde{\mathbf{J}}_m\mathbf{A}^+\mathbf{B})\delta\vec{\chi}_m + \widetilde{\mathbf{J}}_m\mathbf{A}^+\mathbf{W}_2\delta\vec{\chi}_s\right] + \vec{y} \tag{5.44}$$

where $\vec{y} \in \mathcal{N}(\widetilde{\mathbf{J}}_m\widetilde{\mathbf{A}})$. Substituting into (5.43) and rearranging terms, we get (5.38). □

A similar optimization problem can be formulated using joint torque and spatial force as follows

Problem 5.6 *Consider the static force model (5.7). Given desired spatial force* $\vec{f} = \begin{bmatrix} \vec{f}_{dm} \\ \vec{f}_{ds} \end{bmatrix} \in \mathbb{R}^m$ *and desired joint torque* $\vec{\tau}_d$*, find an actual joint torque* $\vec{\tau} \in \mathbb{R}^n$ *such that*

$$\vec{\tau} = \mathbf{J}_m^T\vec{f}_{dm} + \mathbf{J}_s^T\vec{f}_s, \tag{5.45}$$

and

$$\|\mathbf{W}_3(\vec{\tau}-\vec{\tau}_d)\|_2^2+\|\mathbf{W}_4(\vec{f}_s-\vec{f}_{ds})\|_2^2 \tag{5.46}$$

is minimized. $\mathbf{W}_3\in\mathbb{R}^{n\times n}$ *and* $\mathbf{W}_4\in\mathbb{R}^{m_2\times m_2}$ *are weighting matrices.*

The following theorems give solutions to Problem 5.6 for different weighting matrices.

Theorem 5.7 *If* $\mathbf{W}_3$ *and* $\mathbf{W}_4$ *are nonsingular weighting matrices, the unique solution for Problem 5.6 is*

$$\vec{\tau}=\left\{\mathbf{J}_m^T-\mathbf{J}_s^T\begin{bmatrix}\mathbf{W}_3\mathbf{J}_s^T\\ \mathbf{W}_4\end{bmatrix}^+\begin{bmatrix}\mathbf{W}_3\mathbf{J}_m^T\\ \mathbf{0}\end{bmatrix}\right\}\vec{f}_{dm}+\mathbf{J}_s^T\begin{bmatrix}\mathbf{W}_3\mathbf{J}_s^T\\ \mathbf{W}_4\end{bmatrix}^+\begin{bmatrix}\mathbf{W}_3 & \mathbf{0}\\ \mathbf{0} & \mathbf{W}_4\end{bmatrix}\begin{bmatrix}\vec{\tau}_d\\ \vec{f}_{ds}\end{bmatrix}. \tag{5.47}$$

Proof: From (5.45) we have

$$\begin{bmatrix}\mathbf{W}_3(\vec{\tau}-\vec{\tau}_d)\\ \mathbf{W}_4(\vec{f}_s-\vec{f}_{ds})\end{bmatrix}=\begin{bmatrix}\mathbf{W}_3\mathbf{J}_m^T\\ \mathbf{0}\end{bmatrix}\vec{f}_{dm}+\begin{bmatrix}\mathbf{W}_3\mathbf{J}_s^T\\ \mathbf{W}_4\end{bmatrix}\vec{f}_s-\begin{bmatrix}\mathbf{W}_3 & \mathbf{0}\\ \mathbf{0} & \mathbf{W}_4\end{bmatrix}\begin{bmatrix}\vec{\tau}_d\\ \vec{f}_{ds}\end{bmatrix}. \tag{5.48}$$

It is clear that

$$\|\mathbf{W}_3(\vec{\tau}-\vec{\tau}_d)\|_2^2+\|\mathbf{W}_4(\vec{f}_s-\vec{f}_{ds})\|_2^2=\left\|\begin{bmatrix}\mathbf{W}_3(\vec{\tau}-\vec{\tau}_d)\\ \mathbf{W}_4(\vec{f}_s-\vec{f}_{ds})\end{bmatrix}\right\|_2^2. \tag{5.49}$$

Since $\begin{bmatrix}\mathbf{W}_3\mathbf{J}_s^T\\ \mathbf{W}_4\end{bmatrix}$ has full column-rank, $\|\mathbf{W}_3(\vec{\tau}-\vec{\tau}_d)\|_2^2+\|\mathbf{W}_4(\vec{f}_s-\vec{f}_{ds})\|_2^2$ is minimized if and only if

$$\vec{f}_s=-\begin{bmatrix}\mathbf{W}_3\mathbf{J}_s^T\\ \mathbf{W}_4\end{bmatrix}^+\left\{\begin{bmatrix}\mathbf{W}_3\mathbf{J}_m^T\\ \mathbf{0}\end{bmatrix}\vec{f}_{dm}-\begin{bmatrix}\mathbf{W}_3 & \mathbf{0}\\ \mathbf{0} & \mathbf{W}_4\end{bmatrix}\begin{bmatrix}\vec{\tau}_d\\ \vec{f}_{ds}\end{bmatrix}\right\}. \tag{5.50}$$

Substituting (5.50) into (5.45) we get (5.47). □

Theorem 5.8 *If $\mathbf{W}_3$ is invertible and $\mathbf{W}_4 = \mathbf{0}$, the unique solution for Problem 5.6 is*

$$\vec{\tau} = \left[\mathbf{J}_m^T - \mathbf{J}_s^T(\mathbf{W}_3\mathbf{J}_s^T)^+\mathbf{W}_3\mathbf{J}_m^T\right]\vec{f}_{dm} + \mathbf{J}_s^T(\mathbf{W}_3\mathbf{J}_s^T)^+\mathbf{W}_3\vec{\tau}_d. \tag{5.51}$$

Proof: From (5.45) we have

$$\mathbf{W}_3(\vec{\tau} - \vec{\tau}_d) = \mathbf{W}_3\mathbf{J}_m^T\vec{f}_{dm} + \mathbf{W}_3\mathbf{J}_s^T\vec{f}_s - \mathbf{W}_3\vec{\tau}_d. \tag{5.52}$$

Then $\|\mathbf{W}_3(\vec{\tau} - \vec{\tau}_d)\|_2^2$ is minimized if and only if

$$\vec{f}_s = -(\mathbf{W}_3\mathbf{J}_s^T)^+(\mathbf{W}_3\mathbf{J}_m^T\vec{f}_{dm} - \mathbf{W}_3\vec{\tau}_d) + \vec{z} \tag{5.53}$$

where $\vec{z} \in \mathcal{N}(\mathbf{W}_3\mathbf{J}_s^T)$. Since $\mathbf{W}_3$ is invertible, $\mathcal{N}(\mathbf{W}_3\mathbf{J}_s^T) = \mathcal{N}(\mathbf{J}_s^T)$. Thus substituting (5.53) into (5.45) yields (5.51). □

Theorem 5.9 *If $\mathbf{W}_3 = \mathbf{0}$, $\mathbf{W}_4$ is invertible, and $\mathbf{J}_s$ has full row-rank, then the unique solution for Problem 5.6 is*

$$\vec{\tau} = \mathbf{J}_m^T\vec{f}_{dm} + \mathbf{J}_s^T\vec{f}_{ds}. \tag{5.54}$$

Proof: $\|\mathbf{W}_4(\vec{f}_s - \vec{f}_{ds})\|_2^2 = 0$ if and only if $\vec{f}_s = \vec{f}_{ds}$ (since $\mathbf{W}_4$ is invertible) if and only if $\mathbf{J}_s^T\vec{f}_s = \mathbf{J}_s^T\vec{f}_{ds}$ (since $\mathbf{J}_s$ has full row-rank) if and only if $\vec{\tau} = \mathbf{J}_m^T\vec{f}_{dm} + \mathbf{J}_s^T\vec{f}_{ds}$ (from (5.45)). □

5.2.2 Isotropic Motion Planning

In this section, we consider the following problem

Problem 5.10 *Let the differential kinematics model be $\delta\vec{\chi} = \mathbf{J}\delta\vec{\theta}_a$ where $\mathbf{J} \in \mathbb{R}^{m\times n}$ has full rank with $m < n$. Find a transformation matrix $\mathbf{S} \in \mathbb{R}^{n\times m}$ such that, for any given*

$\delta\vec{\chi} \in \mathbb{R}^m$, *the joint space displacement* $\delta\vec{\theta}_a = \mathbf{S}\delta\vec{\chi}$ *generates* $\delta\vec{\chi}$ *(*$\delta\vec{\chi} = \mathbf{JS}\delta\vec{\chi}$*), and the condition number of* $\mathbf{S}$ *is minimized.*

Since $m < n$, here we are dealing with redundant manipulators. $\mathbf{S}$ is an inverse differential kinematics transformation with minimum condition number. We attempt to solve the original problem by utilizing the redundancy in the joint space. In our approach, we restrict the joint space motion to a subspace. Mathematically, this can be written as

$$\delta\vec{\theta}_a = \mathbf{H}\vec{\xi} \tag{5.55}$$

where $\mathbf{H} \in \mathbb{R}^{n\times m}$, $\text{Rank}(\mathbf{H}) = m$, and $\vec{\xi} \in \mathbb{R}^m$ is arbitrary. Thus the Cartesian space motion corresponding to $\delta\vec{\theta}_a$ given by (5.55) is

$$\delta\vec{\chi} = \mathbf{JH}\vec{\xi}. \tag{5.56}$$

To ensure the Cartesian space movements in all m directions, $\mathbf{JH}$ must be full rank. Thus from (5.56), $\vec{\xi}$ can be represented by

$$\vec{\xi} = (\mathbf{JH})^{-1}\delta\vec{\chi}. \tag{5.57}$$

Consequently, (5.55) can be rewritten as

$$\delta\vec{\theta}_a = \mathbf{H}(\mathbf{JH})^{-1}\delta\vec{\chi}. \tag{5.58}$$

It is obvious that $\mathbf{J}\delta\vec{\theta}_a = \mathbf{JH}(\mathbf{JH})^{-1}\delta\vec{\chi} = \delta\vec{\chi}$ for any $\delta\vec{\chi} \in \mathbb{R}^m$.

Based on (5.58), Problem 5.10 is reformulated as

Definition 5.11 *(Isotropic Motion Planning) Given a full rank matrix* $\mathbf{J} \in \mathbb{R}^{m \times n}$ *with* $m < n$*, find a matrix* $\mathbf{H} \in \mathbb{R}^{n \times m}$ *such that* $\mathrm{Rank}(\mathbf{JH}) = \mathrm{m}$*, and* $\mathrm{Cond}[\mathbf{H}(\mathbf{JH}^{-1})]$ *is minimized.*

The problem is solved by the following lemma and theorem.

Lemma 5.12 *Let* $\mathbb{O}^{n \times m}$ *be the set of* $n \times m$ *real matrices with orthonormal columns. Then*

$$\min_{\mathbf{H} \in \mathbb{R}^{n \times m},\ \mathrm{Rank}(\mathbf{JH}) = \mathrm{m}} \mathrm{Cond}[\mathbf{H}(\mathbf{JH})^{-1}] = \min_{\mathbf{H} \in \mathbb{O}^{n \times m},\ \mathrm{Rank}(\mathbf{JH}) = \mathrm{m}} \mathrm{Cond}[\mathbf{H}(\mathbf{JH})^{-1}]. \tag{5.59}$$

Proof: For any $\mathbf{H} \in \mathbb{R}^{n \times m}$, the QR decomposition gives

$$\mathbf{H} = \mathbf{QR} \tag{5.60}$$

where $\mathbf{Q} \in \mathbb{O}^{n \times m}$, $\mathbf{R} \in \mathbb{R}^{m \times m}$ is upper triangular. Since $\mathrm{Rank}(\mathbf{JH}) = \mathrm{m}$, $\mathbf{R}$ is invertible. Thus we have

$$\begin{aligned} \mathbf{H}(\mathbf{JH})^{-1} &= \mathbf{QR}(\mathbf{JQR})^{-1} \\ &= \mathbf{QRR}^{-1}(\mathbf{JQ})^{-1} \\ &= \mathbf{Q}(\mathbf{JQ})^{-1}. \end{aligned} \tag{5.61}$$

This completes the proof. □

Theorem 5.13 *If* $\mathbf{J} \in \mathbb{R}^{m \times n}$ *is full rank,* $m < n$*, and* $\sigma_1 \geq \sigma_2 \geq \cdots \geq \sigma_m > 0$ *are the singular values of* $\mathbf{J}$*, then*

$$\min_{\mathbf{H} \in \mathbb{O}^{n \times m},\ \mathrm{Rank}(\mathbf{JH}) = \mathrm{m}} \mathrm{Cond}[\mathbf{H}(\mathbf{JH})^{-1}] = \frac{\sigma_t}{\sigma_m} \tag{5.62}$$

where $t = \min(n - m + 1, m)$. *One of the minimizers is given by*

$$\mathbf{H} = \left[\mathbf{V}\prod_{i=1}^{t-1}\mathbf{G}_{i,m+i}(\alpha_i)\right]\begin{bmatrix}\mathbf{I}_{m\times m}\\ \\ \mathbf{0}_{(n-m)\times m}\end{bmatrix}. \tag{5.63}$$

$\mathbf{V}$ *is given by the singular value decomposition of* $\mathbf{J}$ *(*$\mathbf{J} = \mathbf{U}\mathbf{\Sigma}\mathbf{V}^T$*).* $\mathbf{G}_{i,j}(\alpha) \in \mathbb{O}^{n\times n}$ *is the Givens rotation matrix with* (i,i)*th and* (j,j)*th entries equal* $\cos(\alpha)$*,* (i,j)*th entry equals* $\sin(\alpha)$*,* (j,i)*th entry equals* $-\sin(\alpha)$*, the other diagonal entries are* 1*s, and the rest entries are* 0*s.* $\alpha_i = \cos^{-1}(\frac{\sigma_m}{\sigma_i})$*.* $\mathbf{I}_{m\times m} \in \mathbb{R}^{m\times m}$ *is the identity matrix.*

Proof: Suppose $m < n < 2m - 1$, for any $\mathbf{H} \in \mathbb{O}^{n\times m}$,

$$[\mathbf{H}(\mathbf{JH})^{-1}]^T\mathbf{H}(\mathbf{JH})^{-1} = (\mathbf{JH})^{-T}(\mathbf{JH})^{-1}. \tag{5.64}$$

Thus

$$\mathrm{Cond}[\mathbf{H}(\mathbf{JH})^{-1}] = \mathrm{Cond}[(\mathbf{JH})^{-1}] = \mathrm{Cond}[\mathbf{JH}] \tag{5.65}$$

for any $\mathbf{H} \in \mathbb{R}^{n\times m}$.

From the Courant-Fischer theorem [13], we have

$$\sigma_{n-k+1}^2 = \min_{S_k\subset\mathbb{R}^n}\max_{\vec{x}\neq\vec{0},\,\vec{x}\in S_k}\frac{\vec{x}^T\mathbf{J}^T\mathbf{J}\vec{x}}{\vec{x}^T\vec{x}} \tag{5.66}$$

$$\sigma_k^2 = \max_{S_k\subset\mathbb{R}^n}\min_{\vec{x}\neq\vec{0},\,\vec{x}\in S_k}\frac{\vec{x}^T\mathbf{J}^T\mathbf{J}\vec{x}}{\vec{x}^T\vec{x}} \tag{5.67}$$

where $S_k \subset \mathbb{R}^n$ denotes a subspace of dimension k, $k = 1, \cdots, n$. Thus

$$\sigma_{n-m+1} = \min_{\mathbf{H}\in\mathbb{O}^{n\times m}}\max_{\vec{y}\neq\vec{0},\,\vec{y}\in\mathbb{R}^m}\frac{\|\mathbf{JH}\vec{y}\|_2}{\|\vec{y}\|_2} \tag{5.68}$$

$$\sigma_m = \max_{\mathbf{H}\in\mathbb{O}^{n\times m}}\min_{\vec{y}\neq\vec{0},\,\vec{y}\in\mathbb{R}^m}\frac{\|\mathbf{JH}\vec{y}\|_2}{\|\vec{y}\|_2} \tag{5.69}$$

This implies that, for any $\mathbf{H} \in \mathbb{O}^{n\times m}$, $\mathrm{Cond}(\mathbf{JH}) \geq \frac{\sigma_{n-m+1}}{\sigma_m}$.

Let the singular value decomposition of $\mathbf{J}$ be given by

$$\mathbf{J} = \mathbf{U}\mathbf{\Sigma}\mathbf{V}^T. \tag{5.70}$$

Substituting equation (5.63) into (5.70) gives

$$\mathbf{JH} = \mathbf{U}\ \mathrm{diag}[\sigma_{\mathrm{m}}, \sigma_{\mathrm{m}}, \cdots, \sigma_{\mathrm{m}}, \sigma_{\mathrm{n-m+1}}, \sigma_{\mathrm{n-m+2}}, \cdots, \sigma_{\mathrm{m}}]. \tag{5.71}$$

Thus

$$\mathrm{Cond}[\mathbf{H}(\mathbf{JH})^{-1}] = \mathrm{Cond}(\mathbf{JH}) = \frac{\sigma_{\mathrm{n-m+1}}}{\sigma_{\mathrm{m}}}. \tag{5.72}$$

Similarly, if $n \geq 2m-1$,

$$\mathrm{Cond}[\mathbf{H}(\mathbf{JH})^{-1}] = \mathrm{Cond}(\mathbf{JH}) = \frac{\sigma_{\mathrm{m}}}{\sigma_{\mathrm{m}}} = 1. \tag{5.73}$$

This completes the proof. □

5.3 Numerical Results

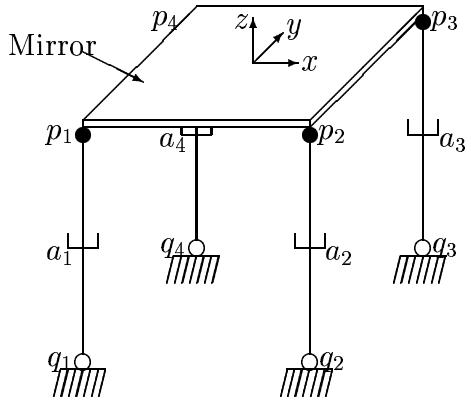

Figure 5.1: Four legged fast steering mirror.

A four legged fast steering mirror, shown in Figure 5.1, is used to demonstrate the ideas presented in this chapter. Four equal length legs are arranged on a cube. a_1, a_2, a_3, and a_4 are linear actuators that can change the length of the legs. p_1, p_2, p_3, and p_4 are spherical joints with 3-DOF's. The 1-DOF hinges (q_1, q_2, q_3, and q_4) at the base can only rotate towards the center of their cube face.

One possible application of a four legged fast steering mirror is fault tolerant pointing. It is not hard to show that the mirror has 3-DOF's (rotation around x and y axes and translation in the z axis). The two rotational DOFs play a dominant role in pointing applications. Thus a four legged fast steering mirror performs prioritized manipulation for pointing applications.

To simplify the computation, we assume the mirror and four legs currently construct a cubic structure with length of edges equal to 1. The optimal velocity mappings defined by (5.35), (5.38), and (5.30) are calculated for two cases:

- There is no actuator failure.
- There is a torque failure in actuator 1.

Let $\delta\vec{\chi} = [\delta\theta_x, \delta\theta_y, \delta z]^T$ be the Cartesian space displacement, $\delta\vec{\theta}_a = [\delta l_1, \delta l_2, \delta l_3, \delta l_4]^T$ be the joint movement. $\delta\theta_x$ ($\delta\theta_y$) is the angle of rotation around x (y) axis, δz is the amount of translation along z axis, δl_i represents the amount of changes in the length of the ith leg. The weighting matrices are identities. $\delta\vec{\theta}_d = \vec{0}$, $\delta\vec{\chi}_d = \vec{0}$.

Case 5.1 *No actuator failure.*

From the geometry shown in Figure 5.1 together with (5.15), we have

$$\mathbf{J} = \begin{bmatrix} -0.5 & -0.5 & 0.5 & 0.5 \\ 0.5 & -0.5 & -0.5 & 0.5 \\ 0.25 & 0.25 & 0.25 & 0.25 \end{bmatrix}. \tag{5.74}$$

Using (5.35), (5.38), and (5.30) we get the same equation

$$\dot{\vec{\theta}}_a = \begin{bmatrix} -0.5 & 0.5 \\ -0.5 & -0.5 \\ 0.5 & -0.5 \\ 0.5 & 0.5 \end{bmatrix} \begin{bmatrix} \delta\theta_x \\ \delta\theta_y \end{bmatrix}. \tag{5.75}$$

This tells us that for a given $\begin{bmatrix} \delta\theta_x \\ \delta\theta_y \end{bmatrix}$, the joint motion defined by (5.75) will produce the given MDOF motion ($\begin{bmatrix} \delta\theta_x \\ \delta\theta_y \end{bmatrix}$) and simultaneously minimizes $\|\delta\vec{\theta}_a\|_2^2$, $\|\delta z\|_2^2$, and $\|\delta\vec{\theta}_a\|_2^2 + \|\delta z\|_2^2$.

Case 5.2 *Torque failure in actuator 1.*

Following the steps in Section 5.1.2, we can get

$$\mathbf{J} = \begin{bmatrix} -1.0 & 1.0 & 0.0 \\ 0.0 & -1.0 & 1.0 \\ 0.5 & 0.0 & 0.5 \end{bmatrix}. \tag{5.76}$$

For a given $\begin{bmatrix} \delta\theta_x \\ \delta\theta_y \end{bmatrix}$, the differential kinematics mapping that minimizes $\|\delta\vec{\theta}_a\|_2^2$ follows from (5.35)

$$\delta\vec{\theta}_a = \frac{1}{3}\begin{bmatrix} -2.0 & -1.0 \\ 1.0 & -1.0 \\ 1.0 & 2.0 \end{bmatrix}\begin{bmatrix} \delta\theta_x \\ \delta\theta_y \end{bmatrix}. \tag{5.77}$$

The differential kinematics mapping that minimizes $\|\delta z\|_2^2$ follows from (5.38)

$$\delta\vec{\theta}_a = \begin{bmatrix} -0.5 & -0.5 \\ 0.5 & -0.5 \\ 0.5 & 0.5 \end{bmatrix}\begin{bmatrix} \delta\theta_x \\ \delta\theta_y \end{bmatrix}. \tag{5.78}$$

The differential kinematics mapping that minimizes $\|\delta\vec{\theta}_a\|_2^2 + \|\delta z\|_2^2$ follows from (5.30)

$$\dot{\vec{\theta}}_a = \frac{1}{8}\begin{bmatrix} -5.0 & -3.0 \\ 3.0 & -3.0 \\ 3.0 & 5.0 \end{bmatrix}\begin{bmatrix} \delta\theta_x \\ \delta\theta_y \end{bmatrix}. \tag{5.79}$$

Chapter 6

Conclusions and Future Work

6.1 Conclusions

The major contributions of this dissertation are summarized as follows

- Decoupling Algorithms

  New decoupling algorithms exploit the properties of the joint space mass-inertia matrix of flexure jointed hexapods, loosen and remove the severe constraints imposed by previous methods on the allowable geometry, workspace, and payload.

- Estimation of the Joint Space Mass-Inertia Matrix

  To apply the new decoupling algorithms, the joint space mass-inertia matrix, $\mathbf{M}_p$, of the flexure jointed hexapod must be known. A new identification algorithm, using an optimization criterion differing from the classical least squares criterion, is proposed to directly estimate $\mathbf{M}_p$ from noisy measurements. The algorithm applies to a class of problems of estimating symmetric and positive definite matrices.

- Decoupled Control

The relationships between different decoupling algorithms and disturbance rejection performance (and robust stability for different uncertainty models) of the corresponding closed-loop system is discussed. We prove that the optimal robustness can be achieved by choosing a unitary decoupling matrix.

- Optimal Jacobians for Prioritized Manipulation

  In many applications, some DOFs in the Cartesian space (operational space) are more important than the rest in performing a task. We call these applications prioritized manipulation. The end-effector's DOFs during a prioritized manipulation can be divided into major DOFs (MDOFs) and secondary DOFs (SDOFs). MDOFs are more important than SDOFs in performing a task. We describe an approach for constructing Jacobians which achieve MDOFs and, at the same time, trade-off SDOFs for some particular reasons such as avoiding obstacles in the workspace, optimizing certain kinematic performance indices, tolerating actuator failures, etc.

6.2 Future Work

- Hexapod Geometry

  By changing the geometry of the hexapod, the isotropic point (with respect to translation or rotation) in the workspace can be adjusted accordingly. The current UW hexapods use a mutually orthogonal geometry [27] (the center of the cube is an isotropic point with respect to translations).

Additional struts can also be introduced to facilitate fault tolerance. The current geometry can't resist torque failure.

- Trajectory Planning

  The techniques in the dissertation give locally optimal Jacobians. To achieve the global optimum, the dynamics of the system must be considered. The calculus of variations may be useful in solving this dynamic problem.

- Sensor Fusion

  Extra sensors, such as a fast steering mirror, could be introduced. This will increase the system bandwidth, expand the possible applications, and further facilitate the tolerance to faults.

Acknowledgments

I would like to thank my advisor Professor John E. McInroy. This work would not have been possible without the guidance and advice of him. John has cultivated a creative atmosphere in our research group, introduced to me exciting research problems, offered me great encouragement, and taught me a lot research and communication skills.

I would like to thank Professors Jerry C. Hamann, Sylvia Hobart, Farhad Jafari, and Robert Kubichek, who have served on my defense committee, for spending much time on reading this dissertation and providing many constructive comments. I am indebted to Professor Siqi Fu, who carefully went through one of my papers. His suggestion greatly improved the quality of the paper and dissertation.

I would also like to thank my colleagues Xiaochun Li, Haomin Lin, Zheng Ma, and Yong Yi. The technical discussions with them at different stages of the dissertation were very rewarding. Special thanks go for Yong Yi. She helped me to complete part of the experiments in the final stage of the dissertation.

I would not have finished this work without the support from my wife Jun Zhang. I would like to thank her for the love and patience she has given to me and her devotion of time to our family.

This work was supported by the Ballistic Missile Defense Organization and Army Research Office under grants DAAG55-98-1-0007 and DAAD 19-00-1-0153.

Bibliography

[1] E. H. Anderson, D. J. Leo, and M. D. Holcomb, "Ultraquiet platform for active vibration isolation," in *Proceedings of the SPIE Smart Structure and Materials Conference,* pp. 436-451, 1996.

[2] J. Baillieul, "Avoiding obstacles and resolving redundancy," in *Proceedings of IEEE Conference on Robotics and Automation,* pp. 1698-1703, 1996.

[3] J. E. Brock, "Optimal Matrices Describing Linear Systems," *AIAA Journal,* 6(1968), pp. 1292-1296.

[4] T. F. Chang and R. V. Dubey, "A weighted least-norm solution based scheme for avoiding joints limits for redundant manipulators," *IEEE Transactions on Robotics and Automation,* vol. 11, no. 2, pp. 286-292, 1995.

[5] F. Chaumette and E. Marchand, "A new redundancy-based iterative scheme for avoiding joint limits application to visual servoing," in *Proceedings of International Conference on Robotics and Automation,* pp. 1720-1725, 2000.

[6] Y. Chen and J. E. McInroy, "Identification and Decoupling Control of Flexure Jointed Hexapods," *Proceedings of IEEE International Conference on Robotics and Automation 2000,* (San Francisco, CA), 1936-1941.

[7] J. J. Craig, *Introduction to Robotics: Mechanics and Control,* Reading, MA: Addison-Wesley, 1986.

[8] K. L. Doty, C. Melchiorri, and C. Bonivento, "A theory of generalized inverse applied to robotics," *The International Journal of Robotics Research,* vol. 12, no. 1, pp. 1-19, 1993.

[9] R. Fletcher, "A nonlinear programming problem in statistics (educational testing)," *SIAM J. Scientific and Statistical Computing*, vol. 2, no. 3, pp. 257–267, September 1981.

[10] R. Fletcher, "Semi-definite matrix constraints in optimization," *SIAM J. Control and Optimization*, vol. 23, no. 4, pp. 493–513, 1985.

[11] Z. J. Geng and L. S. Haynes, "Six degree-of-freedom active vibration control using the Stewart platforms," *IEEE Transactions on Control Systems Technology,* vol. 2, pp. 45-53, March 1994.

[12] Z. J. Geng, G. G. Pan, L. S. Haynes, B. K. Wada, and J. A. Garba, "An intelligent control system for multiple degree-of-freedom vibration isolation," *Journal of Intelligent Material Systems and Structures,* vol. 6, pp. 787-800, November 1995.

[13] G. H. Golub and C. F. Van Loan, *Matrix Computations,* 3rd ed., Johns Hopkins University Press, Baltimore, MD, 1996.

[14] N. J. Higham, "The Symmetric Procrustes Problem," *BIT,* 28(1988), pp. 133-143.

[15] J. M. Hollerbach and K. C. Suh, "Redundancy resolution of manipulators through torque optimization," *IEEE Journal of Robotics and Automation,* vol. RA-3, no. 4, pp. 308-316, 1987.

[16] R. A. Horn and C. R. Johnson, *Matirx Analysis,* Cambridge University Press, 1990.

[17] H. Hu and I. Olkin, "A numerical procedure for finding the positive definite matrix closest to a patterned matrix," *Statistical and Probability Letters*, vol. 12, pp. 511–515, 1991.

[18] H. Hu, "Positive definite constrained least-squares estimation of matrices," *Linear Algebra and it's Applications*, vol. 229, pp. 167–174, 1995.

[19] C. A. Klein and B. E. Blaho, "Dexterity measures for the design and control of kinematically redundant manipulators," *The International Journal of Robotics Research,* vol. 6, no. 2, pp. 72-83, 1987.

[20] K. Kozlowski, *Modelling and Identification in Robotics*, Springer-Verlag, London, 1998.

[21] X. Li, "Simultaneous, Fault-Tolerant Vibration Isolation and Pointing Control of Flexure Jointed Hexapods," *Ph.D Dissertation,* Department of Electrical Engineering, University of Wyoming, 2000.

[22] A. A. Maciejewski and C. A. Klein, "Obstacle avoidance for kinematically redundant manipulators in dynamically varying environments," *The International Journal of Robotics Research,* vol. 4, no. 3, pp. 1095-117, 1985.

[23] A. A. Maciejewski, "Fault tolerant properties of kinematically redundant manipulators," in *Proceedings of IEEE International Conference on Robotics and Automation,* pp. 638-642, 1990.

[24] J. E. McInroy, J. C. Musto, and G. N. Saridis, *Reliable Plan Selection by Intelligent Machines*, World Scientific Publishing, River Edge, NJ, 1995.

[25] J. E. McInroy, J. F. O'Brien, and G. W. Neat, "Precise, fault tolerant pointing using a Stewart platform," *IEEE/ASME Transactions on Mechatronics,* vol. 4, pp. 91-95, March 1999.

[26] J. E. McInroy, "Dynamic Modeling of Flexure Jointed Hexapods for Control Purposes," *IEEE Conference on Control Applications,* (Kona, Hawaii), pp. 508-513, August 1999. (Long version also submitted to *IEEE/ASME Transactions on Mechatronics.*)

[27] J. E. McInroy and J. C. Hamann, "Design and Control of Flexure Jointed Hexapods," *IEEE Transactions on Robotics and Automation,* Vol. 16, No. 4, 372-381, 2000.

[28] S.O.R. Moheimani and G.C. Goodwin, "Special issue on dynamics and control of smart structures," *IEEE Transactions on Control Systems Technology*, vol. 9, no. 1, January 2001.

[29] V. Monteverde and S. Tosunoglu, "Fault tolerance in robotics and mechanical systems: an introduction survey," in *ASME, PD, Proceedings of the 1996 3rd Biennial Joint Conference on Engineering Systems Design and Analysis, ESDA, part 2 (of 9),* vol. 74, pp. 259-264, 1996.

[30] M. J. P. Musgrave, "On the constraints of positive-definite strain energy in anisotropic elastic media," *Quarterly Journal of Mechanics and Applied Mathematics*, vol. 43, no. 4, pp. 605–621, 1990.

[31] Y. Nakamura, H. Hanafusa, and T. Yoshikawa, "Task-priority based redundancy control of robot manipulators," *The International Journal of Robotics Research,* vol. 6, no. 2, pp. 3-15, 1987.

[32] J. F. O'Brien, J. E. McInroy, D. Bodtke, M. Bruch, and J. C. Hamann, "Lessons learned in nonlinear systems and flexible robots through experiments on a 6 legged platform," in *Proceedings of the American Control Conference,* (Philadelphia, PA), pp. 868-872, 1998.

[33] P. Poignet and M. Gautier, "Comparison of weighted least squares and extended Kalman filtering methods for dynamic identification of robots," in *Proc. IEEE Int. Conf. Robotics and Automation.* San Francisco, CA USA, April 2000, pp. 3622–3627.

[34] R. G. Roberts, "Quantifying the local fault tolerance of a kinematically redundant manipulator," in *Proceedings of the American Control Conference,* pp. 1889-1893, 1995.

[35] J. C. Spall, "The information matrix in control: Computation and some applications," in *IEEE Int. Conf. Decision and Control*, December 1999, pp. 2367–2372.

[36] J. Spanos, Z. Rahman, and G. Blackwood, "A soft 6-axis active vibration isolator," in *Proceedings of the American Control Conference,* pp. 412-416, 1995.

[37] J. Sullivan, A. Rahman, R. Cobb, and J. Spanos, "Closed-loop performance of a vibration isolation and suppression system," in *Proceedings of the American Control Conference,* pp. 3974-3978, 1997.

[38] J. Swevers, C. Ganseman, D. Bilgin, J. D. Schutter, and H. V. Brussel, "Optimal robot excitation and identification," *IEEE Transactions Robotics and Automation*, vol. 13, no. 5, pp. 730–740, October 1997.

[39] D. Thayer, J. Vagners, A. Von Flotow, C. Hardham, and K. Scribner, "Six-axis vibration isolation systems using soft actuators and multiple sensors," in *Proceedings of the Annual American Astronautical Society (AAS) Rocky Mountain Guidance and Control Conference,* pp. 497-506, 1998.

[40] S. Van Huffel and J. Vandewalle, *The Total Least Squares Problem: Computational Aspects and Analysis,* SIAM Philadelphia, 1991.

[41] L. Vandenberghe and S. Boyd, "Semidefinite programming," *SIAM Review*, vol. 38, no. 1, pp. 49–95, 1996.

[42] J. T. Wen and L. S. Wilfinger, "Kinematic manipulability of general constrained rigid multibody systems," in *Proceedings of International Conference on Robotics and Automation,* pp. 1020-1025, 1998.

[43] J. T. Wen and L. S. Wilfinger, "Kinematic manipulability of general constrained rigid multibody systems," *IEEE Transactions on Robotics and Automation,* vol. 15, no. 3, pp. 558-567, 1999.

[44] T. Yoshikawa, "Manipulability of robotic mechanisms," *The International Journal of Robotics Research,* vol. 4, no. 2, pp. 3-9, 1985.

[45] L. Zhang, "The H_∞ index of normal transfer function matrices," *Proc. 1993 Region 10 Conference on Computer, Communication, Control and Power Engineering,* Volume 4, pp. 213-217.

[46] K. Zhou and J. C. Doyle, *Essentials of Robust Control,* Prentice Hall, 1997.